Electronic Supplementary Material (ESI) for CrystEngComm.

Supporting Information.

Mutation of position 5 as a crystal engineering tool for a NIR-Emitting DNA-Stabilized Ag_{16} Nanocluster.

Cecilia Cerretani,[a] Jiro Kondo[*,b] and Tom Vosch[*,a]

[a] Department of Chemistry, University of Copenhagen, Universitetsparken 5, 2100 Copenhagen, Denmark. Email: tom@chem.ku.dk

[b] Department of Materials and Life Sciences, Sophia University 102-8554, Tokyo, Japan. E-mail: j.kondo@sophia.ac.jp

MATERIALS AND METHODS

Synthesis. All silver nanoclusters used in this work were synthesized similar to the protocol reported by Bogh et al.[1] Briefly, the hydrated DNA (IDT, standard desalting) was mixed with $AgNO_3$ (99.998%, Sigma Aldrich) in a 10 mM ammonium acetate (NH_4OAc) solution at pH 7.0, prepared in nuclease-free water (IDT). After 15 minutes, the solution was reduced by $NaBH_4$ (99.99%, Sigma Aldrich). The final ratio of [DNA]:[Ag^+]:[BH_4^-] was [1]:[7.5]:[3.75]. The optimal DNA concentration was found to be 25 µM.

HPLC purification. The HPLC purification was performed using a preparative HPLC system from Agilent Technologies with an Agilent Technologies 1260 Infinity fluorescence detector and Agilent Technologies 1100 Series UV-Vis detector, and a Kinetex C18 column (5 µm, 100 Å, 250 × 4.6 mm), equipped with a fraction collector. The mobile phase was a gradient mixture of 35 mM triethylammonium acetate (TEAA) buffer in water (A) and methanol (B). The gradients used for every nanocluster are reported in Table S1.

Time	X5	C5	A5	G5
0-2 min	15% - 20% B	15% - 20% B	15% - 30% B	20% - 40% B
2-22- min	20% - 40% B	20% - 40% B	30% - 50% B	40% - 60% B
22-24 min	40% - 95% B	40% - 95% B	50% - 95% B	60% - 95% B

Table S1. HPLC methods for all mutants.

The flow rate was 1 mL/min for all mutants. Every HPLC run was followed by 6 minutes of washing with 95% TEAA in methanol to remove any remaining sample from the column.

After purification, the solvent was exchanged to 10 mM NH_4OAc by spin-filtration (cut-off = 3 kDa) in order to increase the stability of the sample over time.

Steady-state absorption and emission spectroscopy. The absorption measurements were carried out on a Cary 300 UV-Vis spectrophotometer (Agilent Technologies). Steady-state fluorescence measurements were performed using a FluoTime300 instrument (PicoQuant) with a 507.5 nm pulsed laser (LDH-P-C-510) or a Xenon arc lamp for the steady-state 2D emission versus excitation plots and for the excitation spectra. All fluorescence spectra were corrected for the wavelength dependency of the detector systems, and the 2D maps, as well as the excitation spectra, were additionally corrected for the Xe lamp power.

Quantum yield (Q) determination

Fluorescence quantum yields were determined by a relative method, using a Cresyl Violet in absolute ethanol (Q_R = 0.56) as reference.[2] The absorption and emission spectra were recorded at different concentrations for the samples and the reference. The integrated emission spectra were then plotted as a function of the fraction of absorbed light at the excitation wavelength ($f = 1 - 10^{-A}$). The data was fitted linearly while fixing the y-intercept at zero, and the slopes were used to calculate the quantum yield based on the following equation:

$$Q_S = Q_R \cdot \left(\frac{\alpha_S}{\alpha_R}\right) \cdot \left(\frac{n_S^2}{n_R^2}\right)$$

where *S* and *R* stand for the sample and reference, respectively, *Q* is the quantum yield, α is the slope of the linear regression and *n* is the refractive index of the solvent.

Time-correlated single photon counting. Time-resolved fluorescence and anisotropy measurements were performed using a FluoTime300 instrument from PicoQuant with a 507.5 nm pulsed laser (LDH-P-C-510) as excitation source.

Acquisition and analysis of single decays and TRES data. Time-resolved emission spectra (TRES) were acquired only for X5, A5 and C5 at 5 ^{o}C, 25 ^{o}C and 40 ^{o}C. The emission range was slightly different for every mutation: for X5 it was 650-840 nm, for A5 from 620 to 840 nm, while for C5 was 630-820 nm. For all the mutants, the wavelength step was 5 nm, and an integration time of 30 s per decay was used in order to achieve at least 10,000 counts in the maximum at the emission maximum. The analysis of time-resolved data was performed with Fluofit v.4.6 from PicoQuant. All decays were fitted globally with a bi- or tri-exponential reconvolution model including scattered light contribution and the IRF (instrument response function). The obtained TRES were corrected for the detector efficiency and transformed to wavenumber units by multiplying with the Jacobian factor ($10^7/v^2$).[3] TRES were interpolated with a spline function using the built-in *spaps* MATLAB function with a tolerance of 10^{-10} (forcing the interpolated curve to go through the data points). The curves were interpolated using wavenumber steps equivalent to 0.001 nm wavelength steps. The emission maxima were taken as the maxima of the interpolated TRES. The average decay time $<\tau>$ of every decay was calculated as the intensity-weighted average decay time. The overall intensity-weighted average decay time $<\tau_\omega>$ was calculated as the average of $<\tau>$ over the emission spectra weighted by the steady-state intensity.[4]

In the case of G5, the presence of two emitters with overlapping emission spectra prevented the acquisition of TRES data. However, single decays at the corresponding emission maxima for G5 RED (λ_{em}=600 nm) and G5-NIR (λ_{em}=730 nm) were carried out at the same temperatures. The integration time was 10, 15 or 20 s, in order to reach at least 10,000 counts in the maximum. The analysis of time-resolved data was performed with the same Fluofit v.4.6 software from PicoQuant. All decays were fitted globally with a bi-, tri- or tetra-exponential reconvolution model including scattered light contribution and the IRF (instrument response function). The average decay time $<\tau>$ was calculated as the intensity-weighted average decay time at a specific wavelength.

Acquisition and analysis of time-resolved anisotropy data. Time-resolved anisotropy measurements were carried out by exciting the sample with vertically polarized light at 507.5 nm (LDH-P-C-510) and acquiring both vertically and horizontally polarized fluorescence intensity decays. The decays were fitted by Fluofit v.4.6 from PicoQuant. A multi-exponential and a mono-exponential reconvolution model were used, respectively, for the decay time and the rotational correlation time (θ), including the IRF. The Perrin equation[5] $\theta=\eta V_{hydro}/k_BT$, where η is the dynamic viscosity of the solvent, V_{hydro} is the hydrodynamic volume of the species and k_BT is the product between the Boltzmann constant (k_B) and the absolute temperature (T), allowed us to calculate the hydrodynamic volume of the clusters. For simplicity, the Perrin model assumes that the investigated species is spherical. Time-resolved fluorescence and anisotropy measurements were performed at three different temperatures: 5^{o}C, 25^{o}C and 40^{o}C, for X5, A5, C5 and G5-NIR.

Crystal growth.

Crystals were grown in an incubator at 293 K by the hanging-drop vapor-diffusion method. 0.2 µL of cluster solution was mixed with 0.2 µL of crystallization buffer and equilibrated against 250 µL of a reservoir solution. The crystallization conditions used for X-ray diffraction measurements are summarized in Table S2.

Table S2. Crystallization conditions for all mutants.

Crystal	**A5**	**C5**	**G5-NIR**	**X5**
PDB-ID	7BSE	7BSF	7BSG	7BSH
Sample solution				
DNA-Ag_{16} nanocluster [DNA]	253 µM	300 µM	184 µM	433 µM
Crystallization solution				
3-(N-morpholino)propanesulfonic acid (MOPS) (pH 7.0)	50 mM	50 mM	50 mM	50 mM
Spermine	10 mM	10 mM	10 mM	10 mM
Calcium nitrate	500 mM	100 mM	100 mM	10 mM
2-Methyl-2,4-pentanediol (MPD)	-	10%	-	10%
Polyethylene glycol (PEG) 3350	10%	-	10%	-
Reservoir solution				
2-Methyl-2,4-pentanediol (MPD)	-	40%	-	40%
Polyethylene glycol 3350 (PEG)	40%	-	40%	-

A crystal from every well-plate was scooped by a nylon cryoloop (Hampton Research) and then flash-frozen in liquid nitrogen prior to the X-ray experiment.

X-Ray data collection. X-ray data were collected at 100 K with synchrotron radiation at the BL-17A beamline in the Photon Factory (Tsukuba, Japan). A 0.98 Å X-ray beam, the default wavelength in the BL-17A beamline, was chosen for the data collections. In accordance with the experimental condition in our previous study,[6] the data set were collected using 1° oscillation with 0.1 s exposure per frame to limit radiation damage. No significant radiation damage was observed for all the crystals.

Structure determination and refinement. The data set were processed by the program XDS.[7] The initial phases were determined with AutoMR from the Phenix suite[8-9] by molecular replacement using the original T5 structure as a model (PDB-ID = 6JR4). A molecular models were constructed by using the program Coot.[10-11] The atomic parameters were refined by using the program phenix.refine of the Phenix suite at maximum resolutions of 1.5 (A5), 1.1 (C5), 2.2 (G5-NIR) and 1.2 (X5) Å, respectively.[8] For the C5 and X5 mutants, hydrogen atoms were included in the structure refinements and anisotropic b-factors were applied for all atoms except for the hydrogen atoms due to the atomic resolution. Statistics of data collection and structure refinement are summarized in Tables S3 and S4.

Spectroscopic characterization. Bright-field and fluorescence images were recorded on an inverted Olympus IX71 equipped with an Olympus CPlanFL N 10x objective. For the bright-field images, a white light source and a 30:70 beam splitter (XF122 Omega Optical) as dichroic were used. For the fluorescence images, an X-Cite Series 120Q light source was used in combination with an Olympus BP510-550 excitation filter, Olympus BA590 emission filter and Semrock FF580-FDi01 dichroic filter. All images (Figures 4, S21, S22, S23, S24) were recorded with a SONY XPERIA XZ mobile phone camera.

Confocal spectra from individual crystals were recorded on an inverted confocal microscope (Olympus IX71) equipped with an Olympus CPlanFL N 10x objective. 520 nm light from a continuum laser (SuperK EXTREME EXB-6 with SuperK SELECT AOTF wavelength selector) was used in combination with a Semrock FF01-520/5 and Olympus BP510-550 excitation filter, Olympus BA590 emission filter and Semrock FF580-FDi01 dichroic filter. The emission spectra were recorded with a spectrometer (Princeton Instruments SPEC-10:100B/LN_eXcelon CCD camera with SP 2356

polychromator, 300 grooves/mm). X-axis calibration was performed using the emission lines of a neon spectral lamp (6032 Newport). Y-axis calibration was done by measuring a reference spectrum on an intensity-calibrated Fluotime300 (PicoQuant) instrument. Emission spectra were recorded with 10 s integration time. The emission maxima were estimated by fitting the spectra with multiple Gaussian functions. Fluorescence decay time measurements were performed on the same inverted confocal microscope (Olympus IX71) equipped with an Olympus CPlanFL N 10x objective. 520 nm light from a continuum laser (SuperK EXTREME EXB-6 with SuperK SELECT AOTF wavelength selector) was used as excitation source. The excitation source power for emission spectra and fluorescence decays was measured on the top of the samples and it is reported in the captions of the corresponding spectra and decay figures. The fluorescence signal was detected by an avalanche photodiode (Perkin-Elmer CD3226) connected to a single photon counting module (Becker & Hickl SPC-830). A 30:70 beam splitter (XF122 Omega Optical) was used as dichroic mirror and two long-pass filters were added in the detection path (LP 515 Delta and BLP02-561R-25 Semrock). All fluorescence decays were tail-fitted with a bi-exponential model.

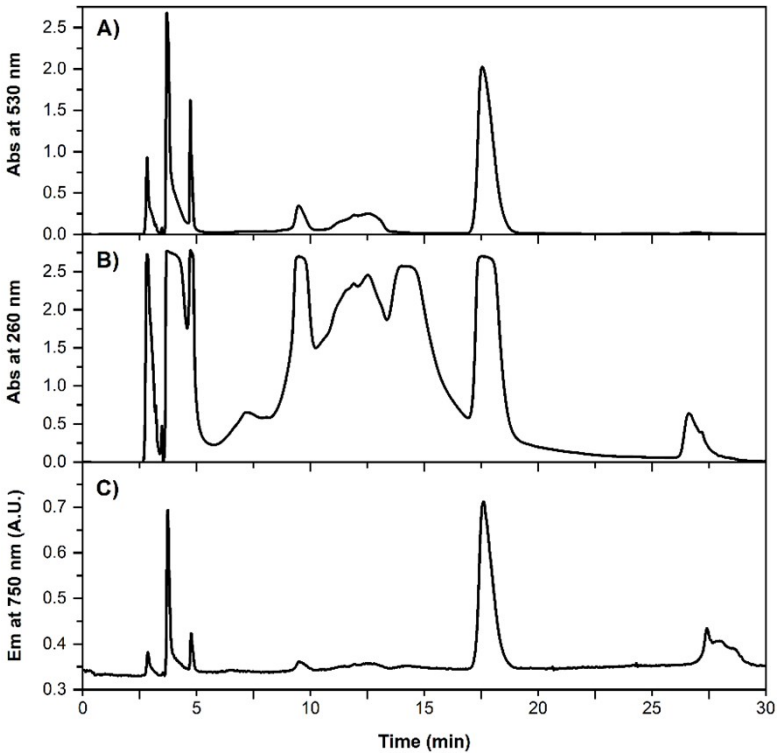

Figure S1. HPLC chromatograms of X5 **A)** monitoring the absorption of X5 at 530 nm; **B)** monitoring the DNA absorption at 260 nm; **C)** monitoring the emission of X5 at 750 nm (exciting at 530 nm). The fraction collected around 17.5 min (≈35%-36% TEAA in MeOH) is the sample described in the manuscript.

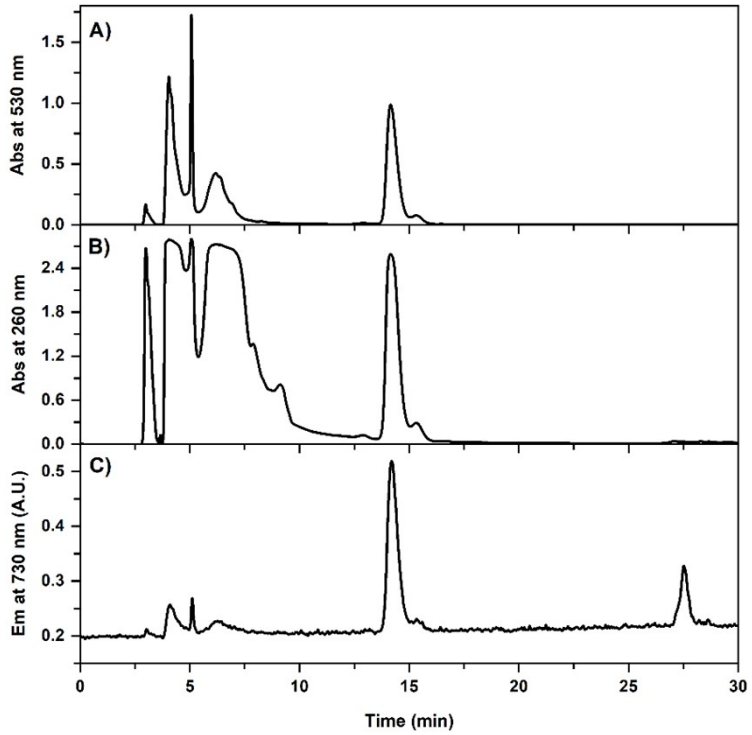

Figure S2. HPLC chromatograms of A5 **A)** monitoring the absorption of A5 at 530 nm; **B)** monitoring the DNA absorption at 260 nm; **C)** monitoring the emission of A5 at 730 nm (exciting at 530 nm). The fraction collected around 14 min (≈42% TEAA in MeOH) is the sample described in the manuscript.

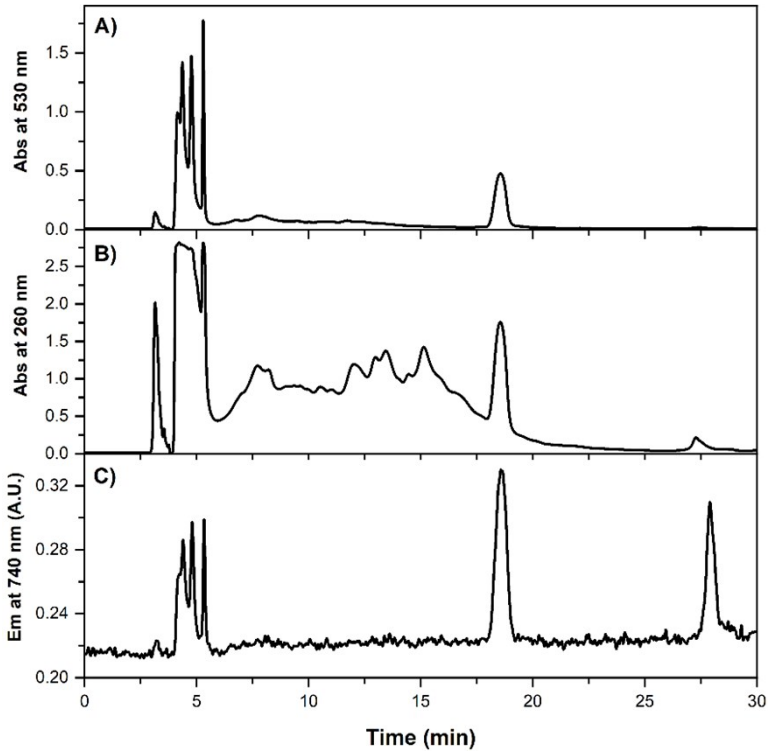

Figure S3. HPLC chromatograms of C5 **A)** monitoring the absorption of C5 at 530 nm; **B)** monitoring the DNA absorption at 260 nm; **C)** monitoring the emission of C5 at 740 nm (exciting at 530 nm). The fraction collected around 18.5 min (≈36%-37% TEAA in MeOH) is the sample described in the manuscript.

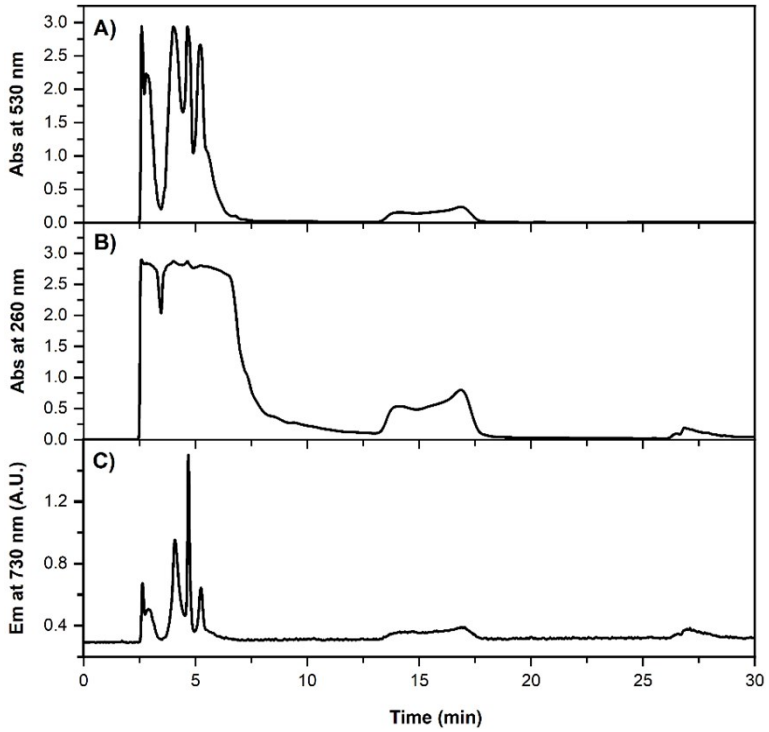

Figure S4. HPLC chromatograms of G5 **A)** monitoring the absorption of G5 at 530 nm; **B)** monitoring the DNA absorption at 260 nm; **C)** monitoring the emission of G5 at 730 nm (exciting at 530 nm). The fraction collected between 14 and 17 min (≈52%-55% TEAA in MeOH) is the sample described in the manuscript.

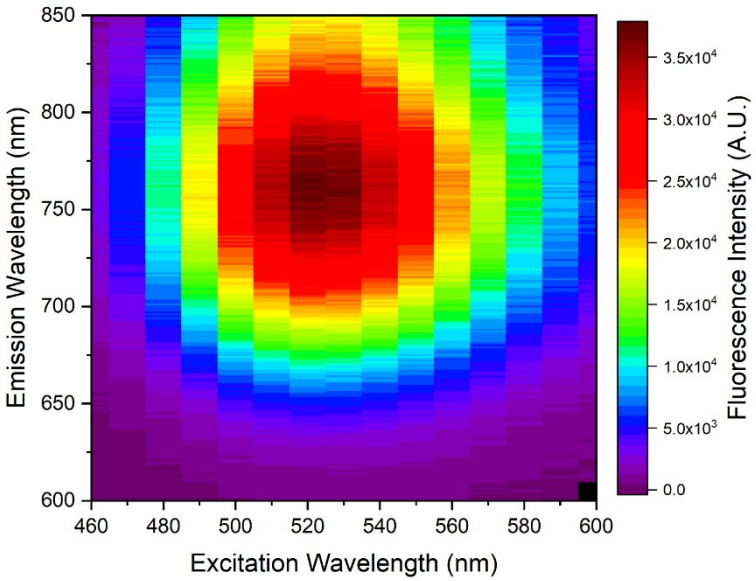

Figure S5. 2D emission vs excitation plot of X5 in 10 mM NH_4OAc solution. The data was recorded at room temperature.

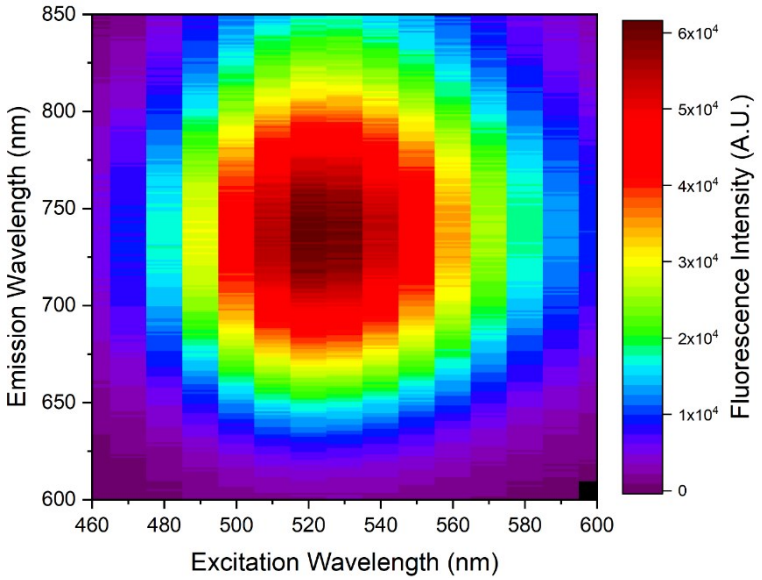

Figure S6. 2D emission vs excitation plot of A5 in 10 mM NH_4OAc solution. The data was recorded at room temperature.

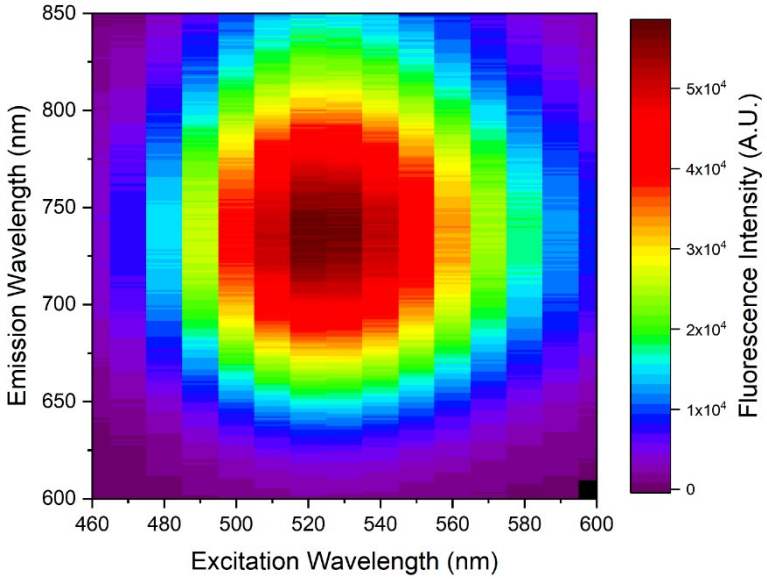

Figure S7. 2D emission vs excitation plot of C5 in 10 mM NH_4OAc solution. The data was recorded at room temperature.

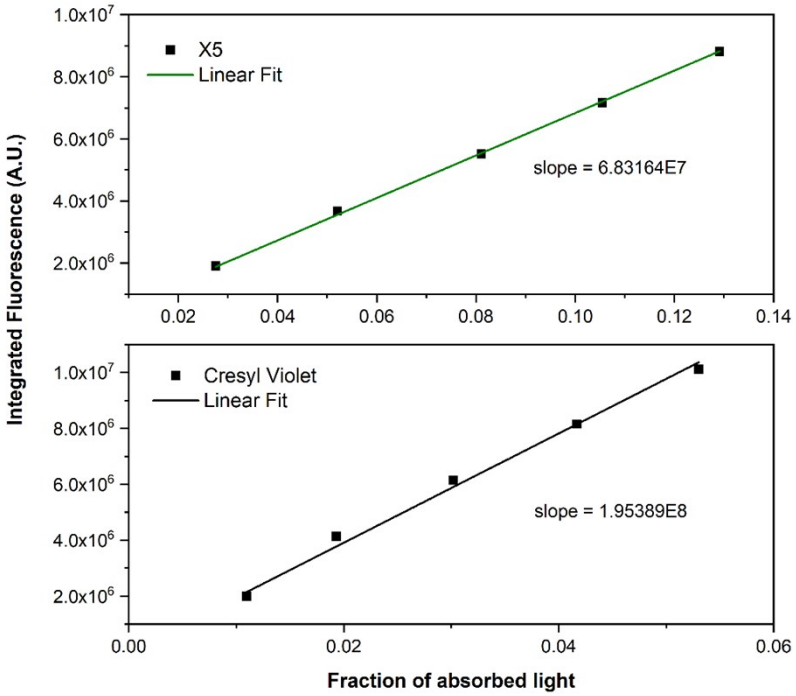

Figure S8. Zero-intercept linear fits of the integrated fluorescence counts plotted against the fraction of absorbed light for X5 (in 10 mM NH_4OAc) and Cresyl Violet (in absolute ethanol) at 25 °C. The resulting slopes were used to determine the fluorescence quantum yield. The fraction of absorbed light is defined as $f = 1\text{-}10^{-A}$, where A is the absorbance at the excitation wavelength.

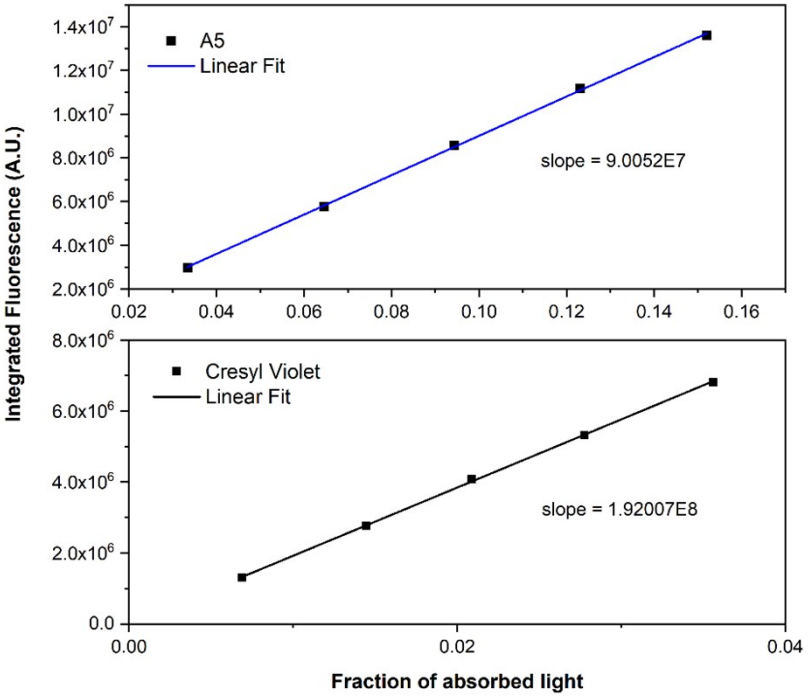

Figure S9. Zero-intercept linear fits of the integrated fluorescence counts plotted against the fraction of absorbed light for A5 (in 10 mM NH_4OAc) and Cresyl Violet (in absolute ethanol) at 25 °C. The resulting slopes were used to determine the fluorescence quantum yield. The fraction of absorbed light is defined as $f = 1\text{-}10^{-A}$, where A is the absorbance at the excitation wavelength.

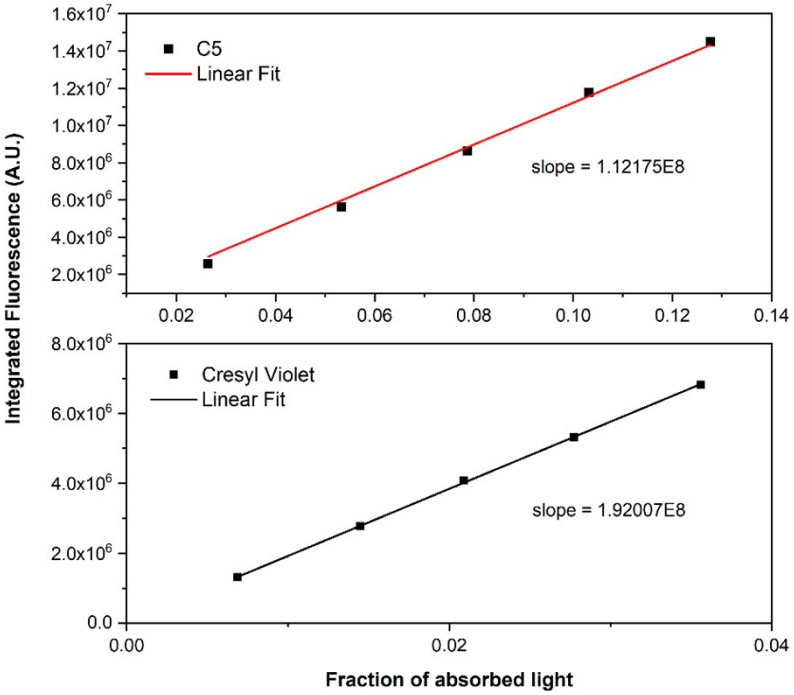

Figure S10. Zero-intercept linear fits of the integrated fluorescence counts plotted against the fraction of absorbed light for C5 (in 10 mM NH_4OAc) and Cresyl Violet (in absolute ethanol) at 25 °C. The resulting slopes were used to determine the fluorescence quantum yield. The fraction of absorbed light is defined as $f = 1\text{-}10^{-A}$, where A is the absorbance at the excitation wavelength.

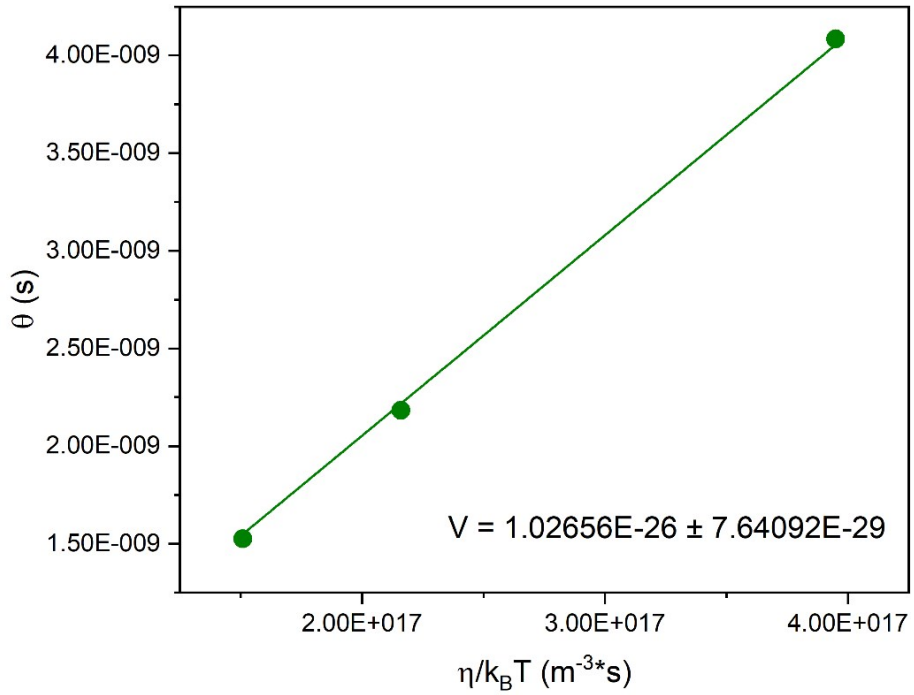

Figure S11. Linear fit of the rotational correlation times (θ) as a function of η/k_BT for X5 in 10 mM NH_4OAc. Data points were collected 5 °C, 25 °C and 40 °C. The slope (V) represents the hydrodynamic volume.

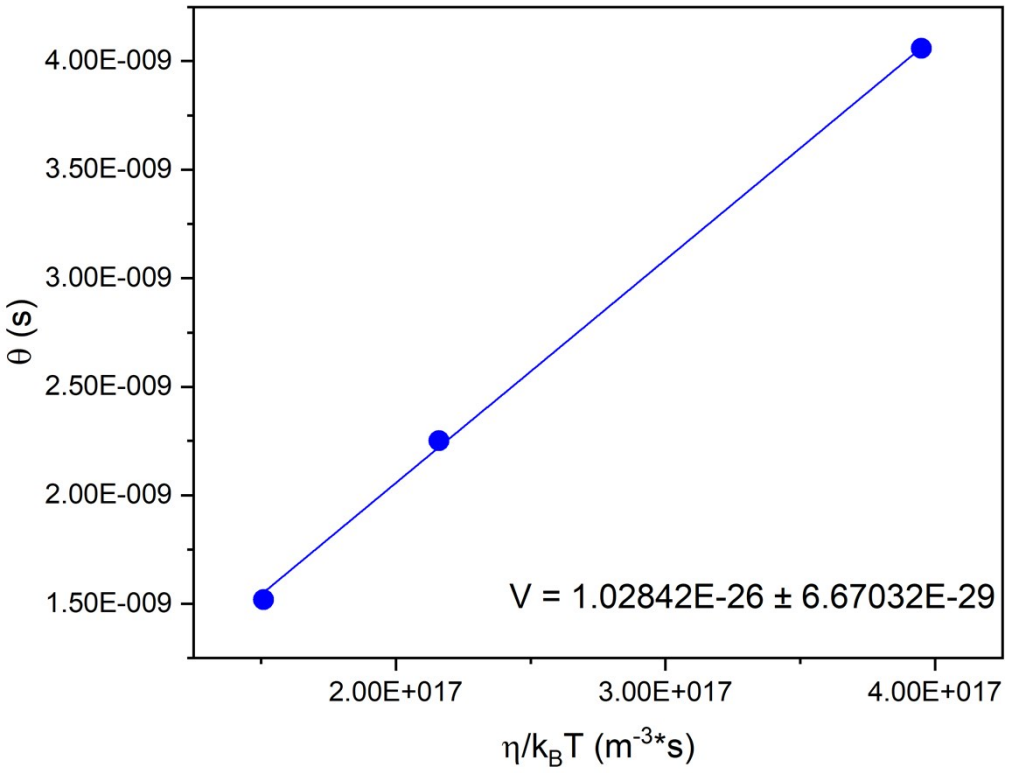

Figure S12. Linear fit of the rotational correlation times (θ) as a function of η/k_BT for A5 in 10 mM NH_4OAc. Data points were collected 5 °C, 25 °C and 40 °C. The slope (V) represents the hydrodynamic volume.

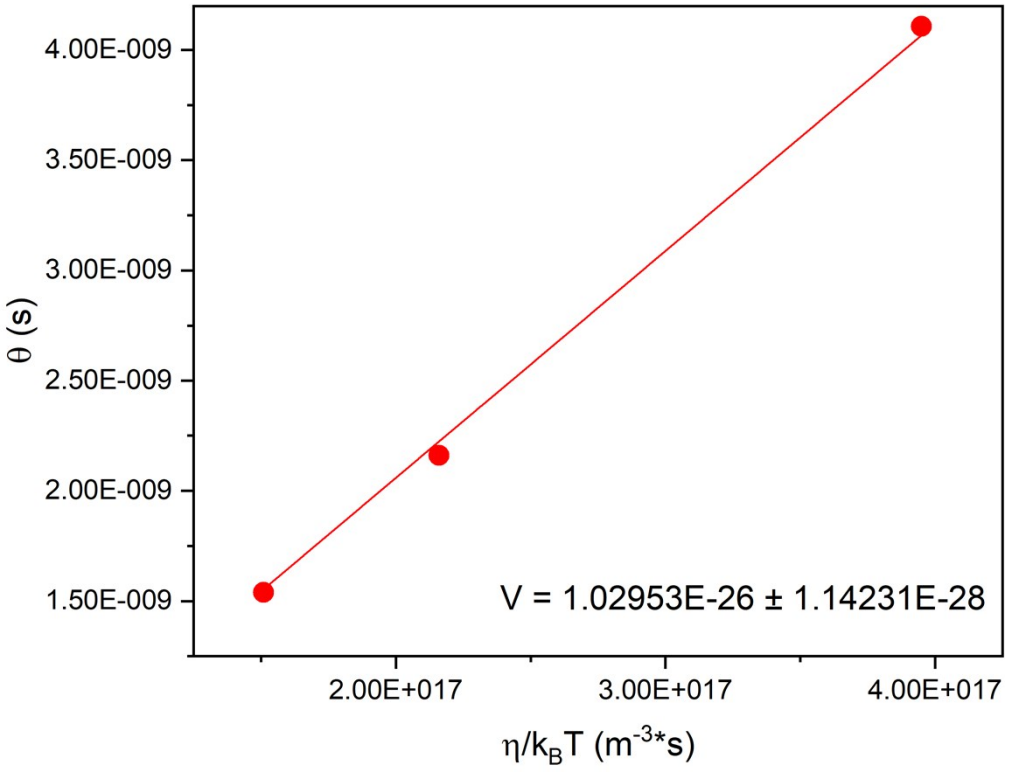

Figure S13. Linear fit of the rotational correlation times (θ) as a function of η/k_BT for C5 in 10 mM NH_4OAc. Data points were collected 5 °C, 25 °C and 40 °C. The slope (V) represents the hydrodynamic volume.

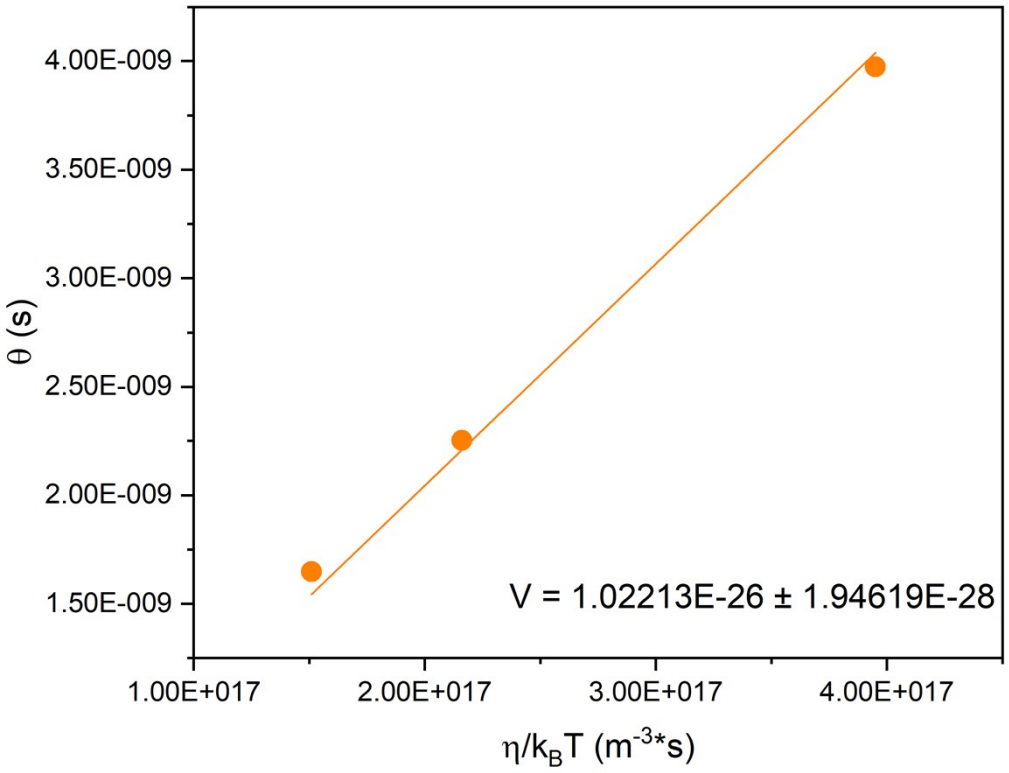

Figure S14. Linear fit of the rotational correlation times (θ) as a function of η/k_BT for G5-NIR in 10 mM NH_4OAc. Data points were collected 5 °C, 25 °C and 40 °C. The slope (V) represents the hydrodynamic volume.

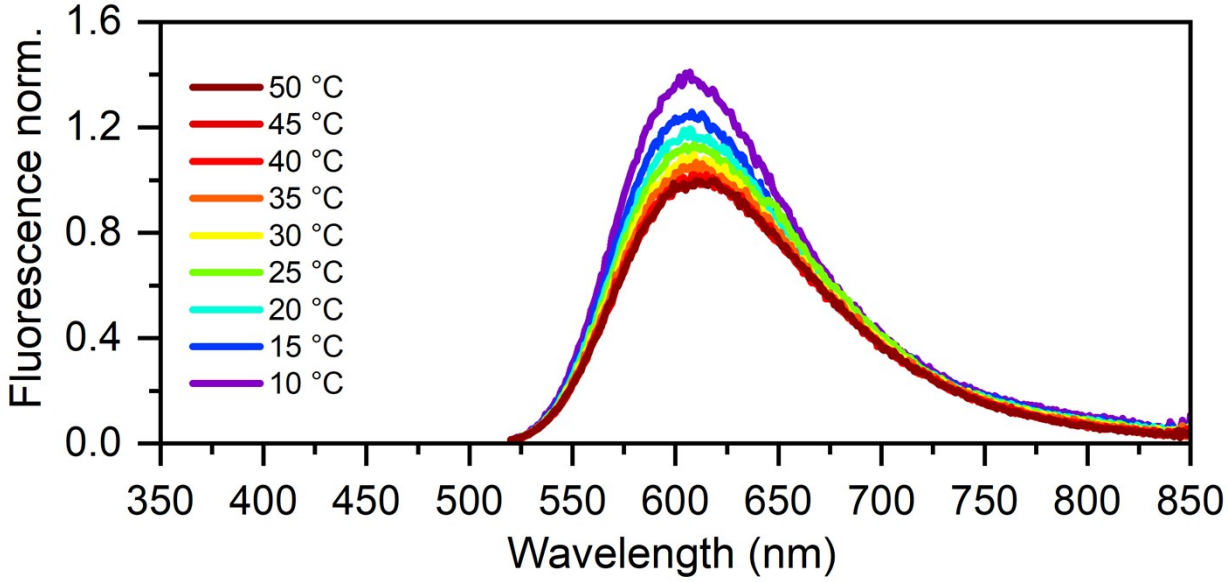

Figure S15. Emission spectra (λ_{exc}=507.5 nm) corresponding to the cooling cycle of G5 after the first heating cycle, shown in Figure 2B.

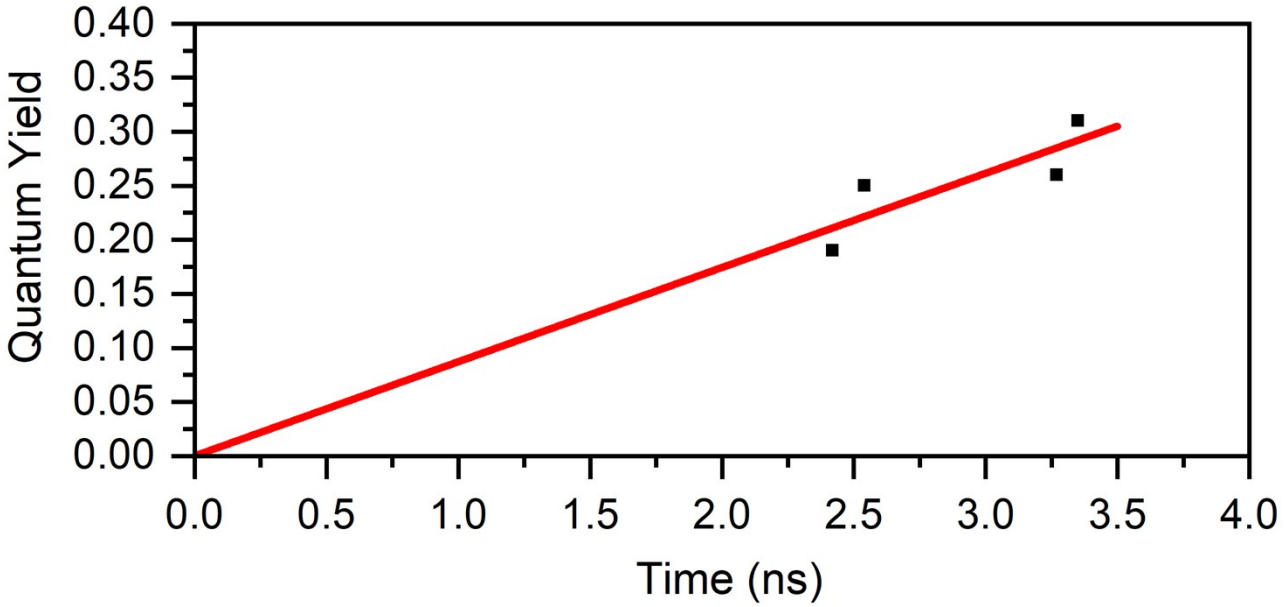

Figure S16: Quantum yield as a function of decay time for T5, X5, A5 and C5 in 10 mM NH_4OAc solution at 25°C. Data points were fitted with a line intersecting (0,0).

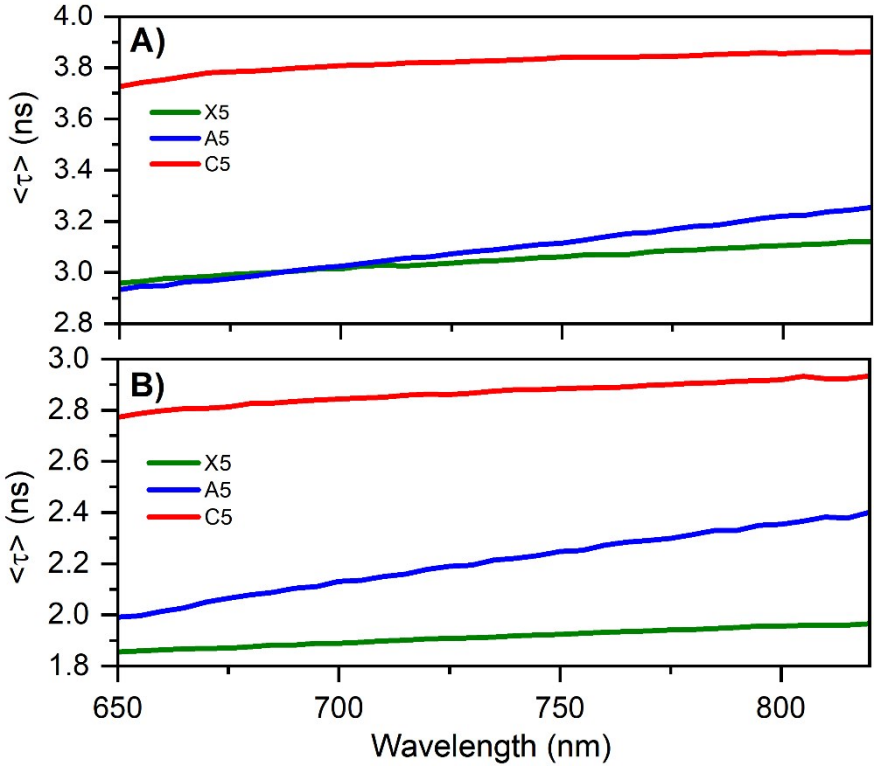

Figure S17: Intensity-weighted average decay time as a function of detection wavelength for X5, A5 and C5 at **A)** 5 °C and **B)** 40 °C. The plot at 25 °C can be found in Figure 3.

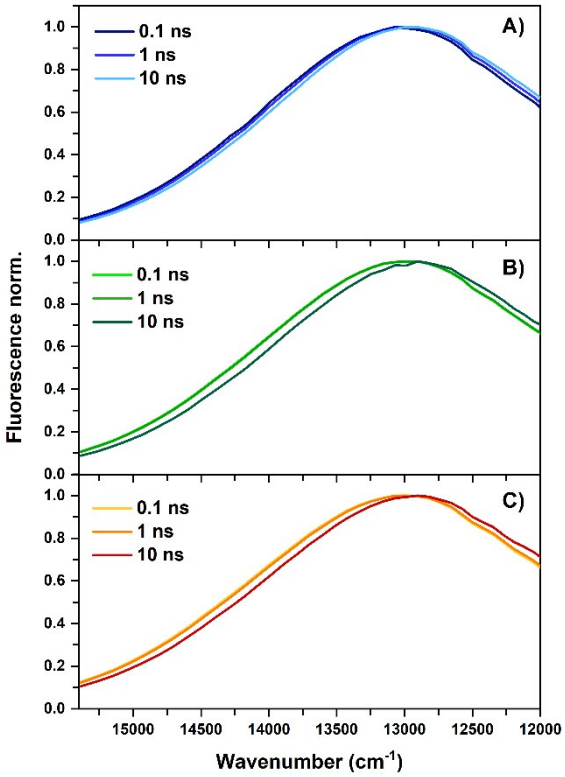

Figure S18: TRES of X5 in 10 mM NH_4OAc at **A)** 5 °C, **B)** 25 °C, **C)** 40 °C.

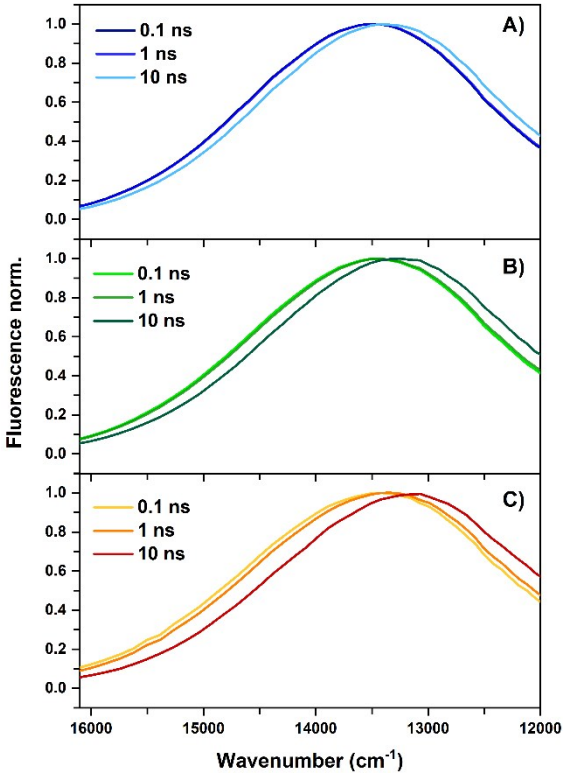

Figure S19: TRES of A5 in 10 mM NH_4OAc at **A)** 5 °C, **B)** 25 °C, **C)** 40 °C.

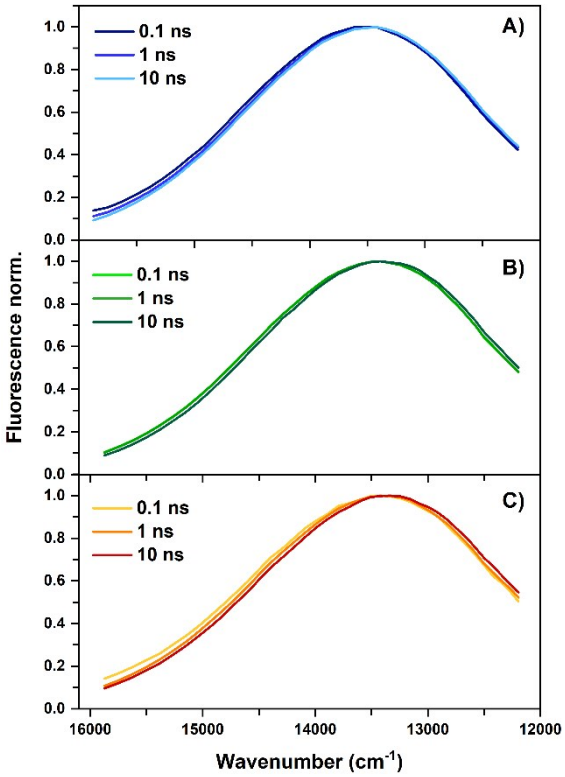

Figure S20: TRES of C5 in 10 mM NH_4OAc at **A)** 5 ^oC, **B)** 25 ^oC, **C)** 40 ^oC.

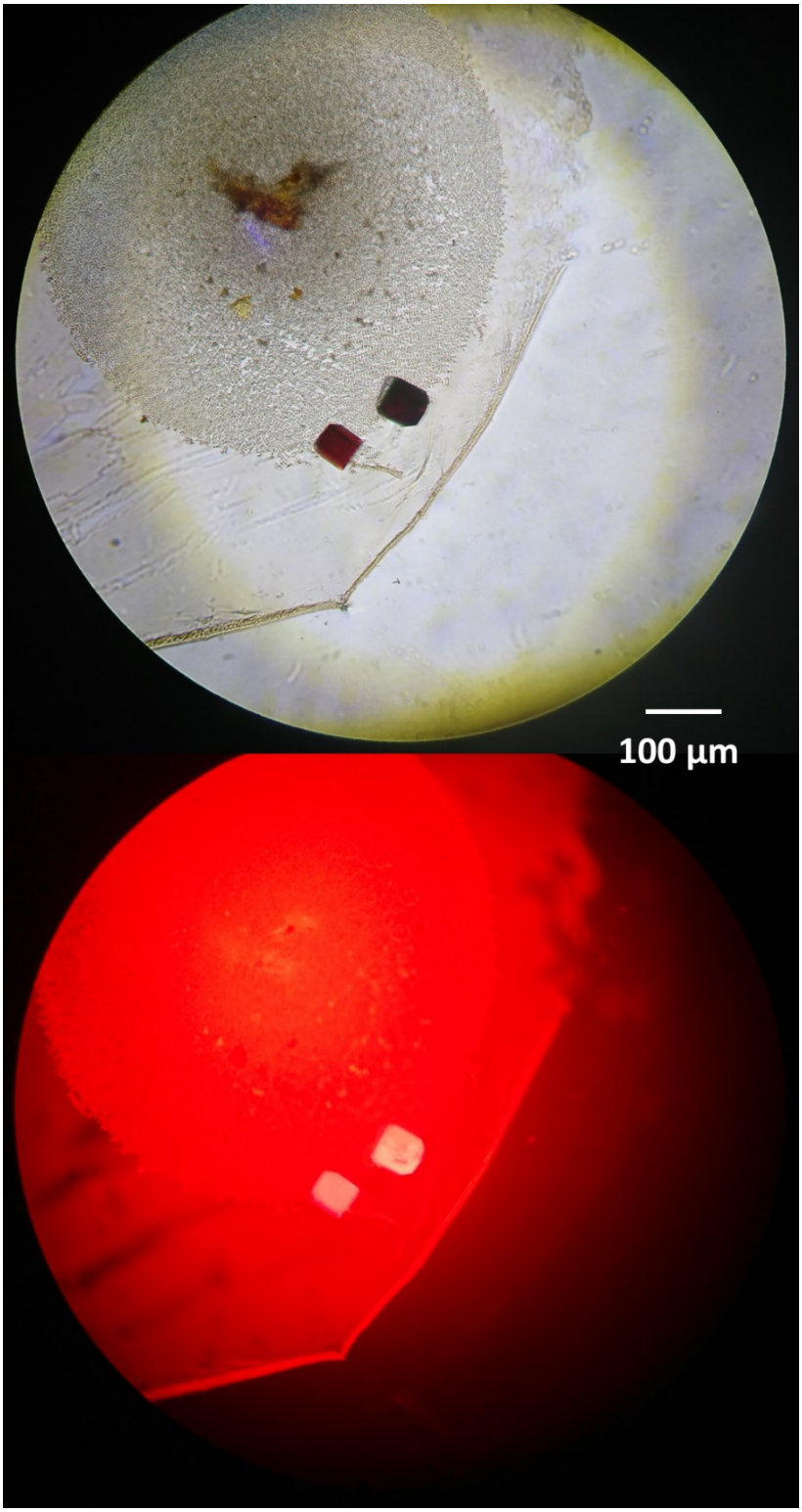

Figure S21: X5 crystals. 1 µL of X5 solution was mixed with 1 µL of crystallization buffer composed by 10% MPD, 10 mM spermine, 50 mM MOPS (pH=7) and 10 mM $Ca(NO_3)_2$. Bright field image of crystallization well at 10x magnification and fluorescence image of the same region. The fluorescence intensity of the crystals saturated (white color) the intensity of the camera. Images were taken 5 months and a half after start of crystallization.

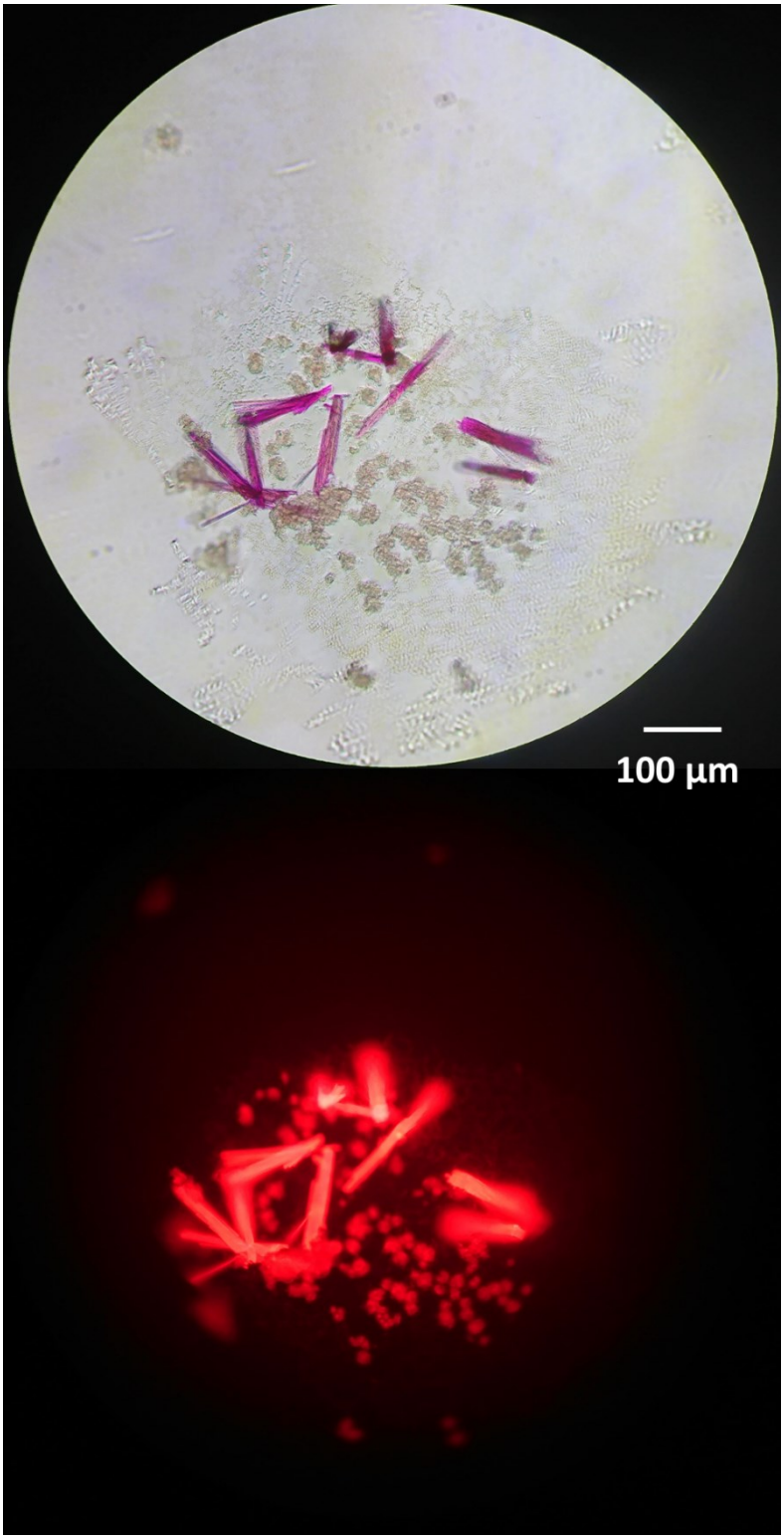

Figure S22: A5 polycrystals. 1 µL of A5 solution was mixed with 1 µL of crystallization buffer composed by 10% PEG, 10 mM spermine, 50 mM MOPS (pH=7) and 500 mM $Ca(NO_3)_2$. Bright field image of crystallization well at 10x magnification and fluorescence image of the same region. The fluorescence intensity of the crystals saturated (white color) the intensity of the camera. Images were taken circa 5 months and a half after start of crystallization.

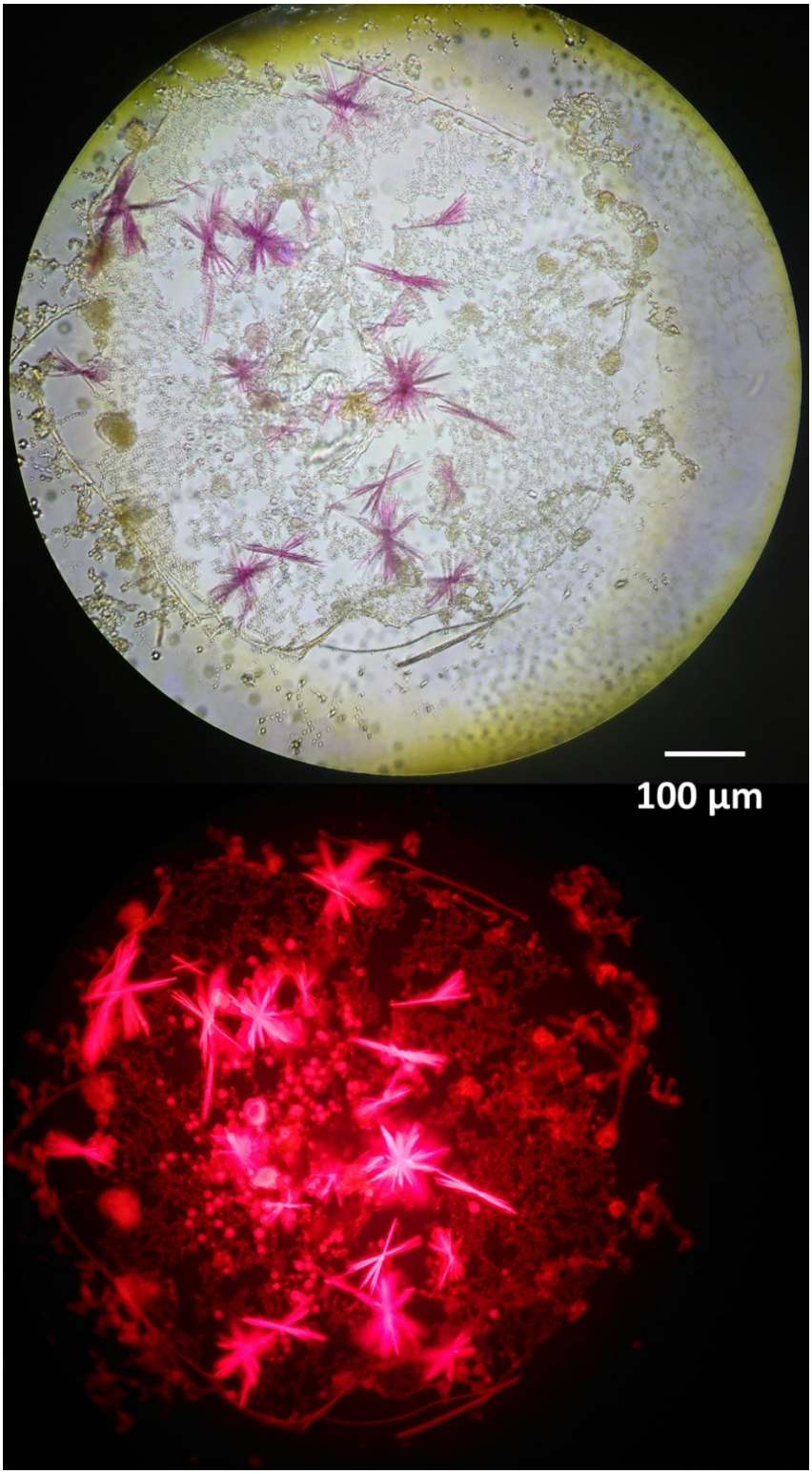

Figure S23: C5 polycrystals1 µL of C5 solution was mixed with 1 µL of crystallization buffer composed by 10% MPD, 10 mM spermine, 50 mM MOPS (pH=7) and 100 mM $Ca(NO_3)_2$. Bright field image of crystallization well at 10x magnification and fluorescence image of the same region. The fluorescence intensity of the crystals saturated (white color) the intensity of the camera. Images were taken roughly 6 months after start of crystallization.

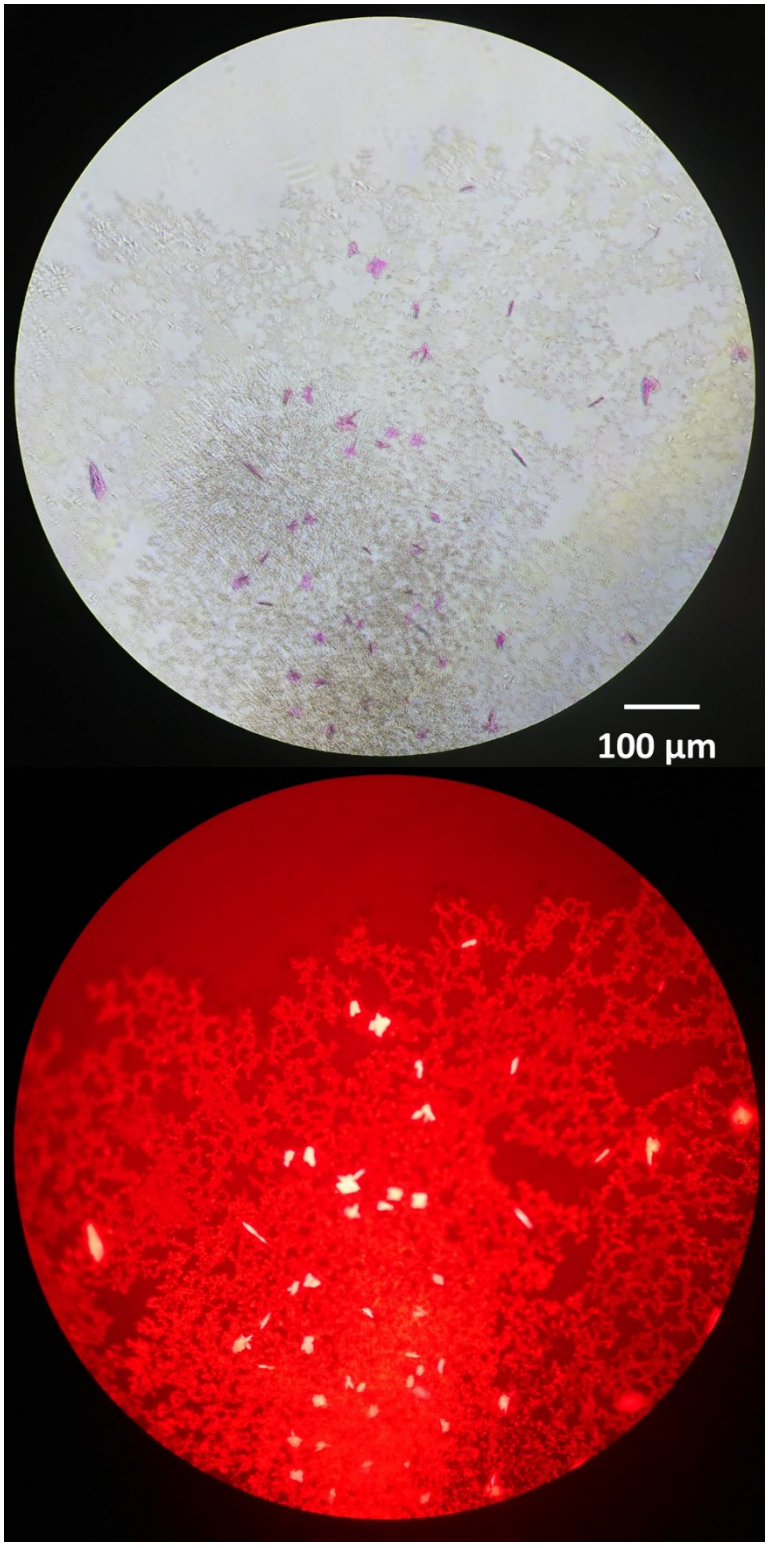

Figure S24: G5 polycrystals. 1 µL of G5 solution was mixed with 1 µL of crystallization buffer composed by 10% PEG, 10 mM spermine, 50 mM MOPS (pH=7) and 10 mM $Ca(NO_3)_2$. Bright field image of crystallization well at 10x magnification and fluorescence image of the same region. The fluorescence intensity of the crystals saturated (white color) the intensity of the camera. Images were taken approximately 3 months after start of crystallization.

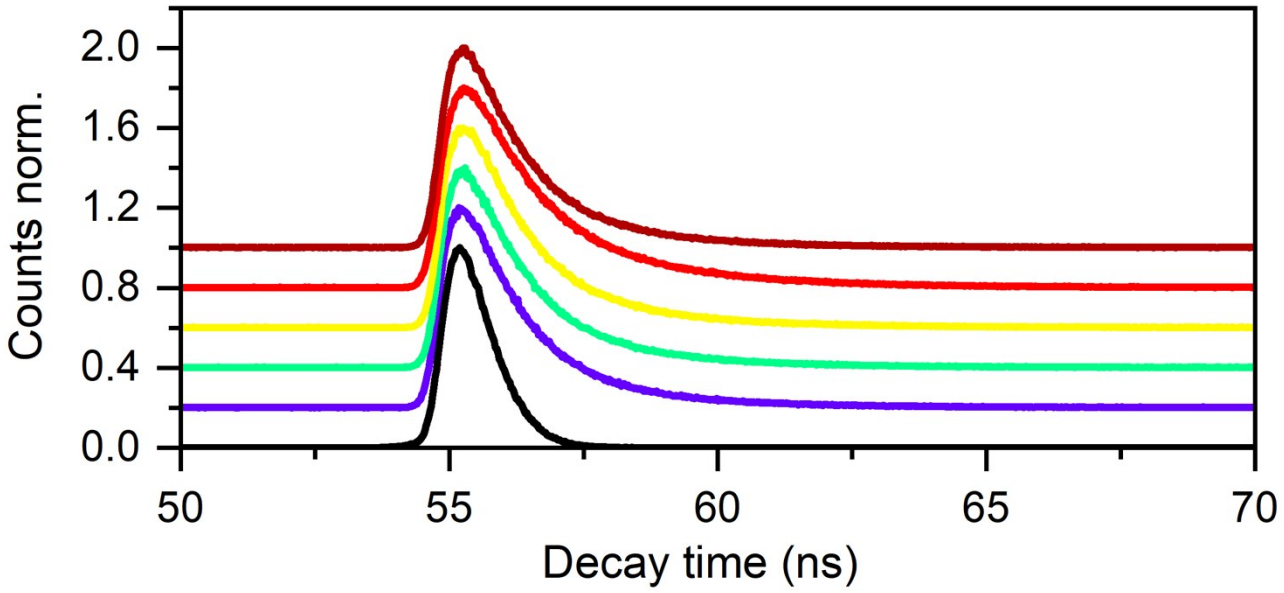

Figure S25: Fluorescence decay time measurements of five different positions of X5 crystals, excited at 520 nm (45 nW). The colored curves are the fluorescence decays, while the black curve is the instrument response function (IRF). Every decay was tail-fitted with 2 exponents, and intensity-weighted average decay times of 1.61, 1.64, 1.65, 1.94, and 1.53 ns were found. The average decay time (1.68 ns) obtained from these five values is used in the manuscript.

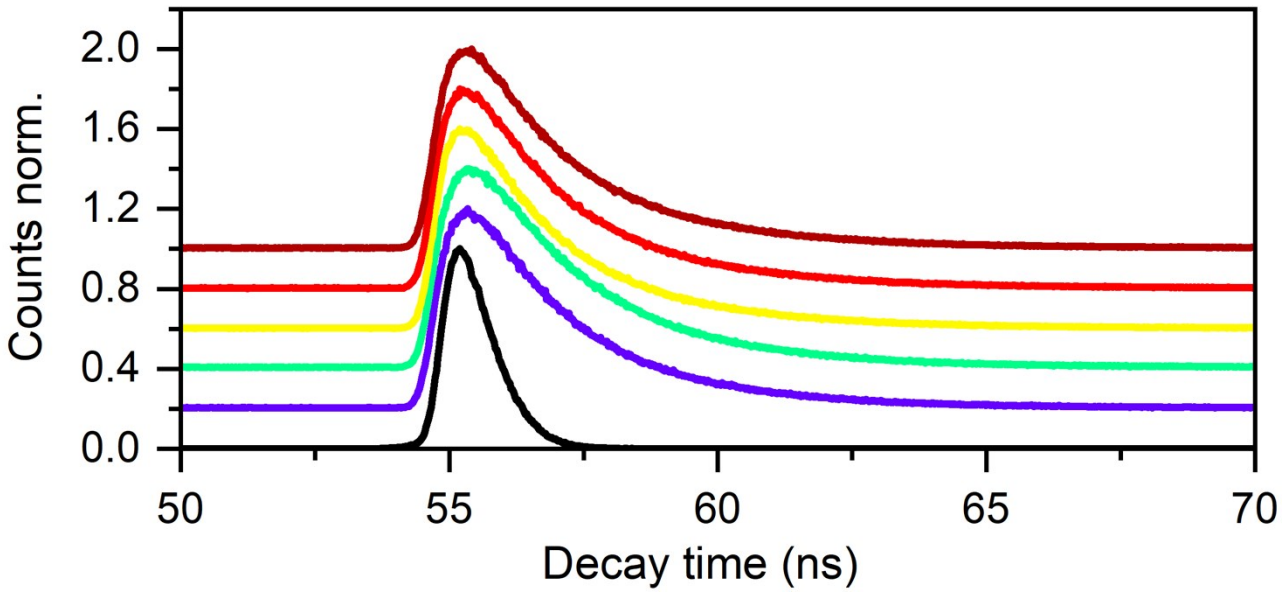

Figure S26: Fluorescence decay time measurements of five different positions of A5 crystals, excited at 520 nm (45 nW). The colored curves are the fluorescence decays, while the black curve is the instrument response function (IRF). Every decay was tail-fitted with 2 exponents, and intensity-weighted average decay times of 2.22, 2.30, 2.23, 2.29, and 2.27 ns were found. The average decay time (2.26 ns) obtained from these five values is used in the manuscript.

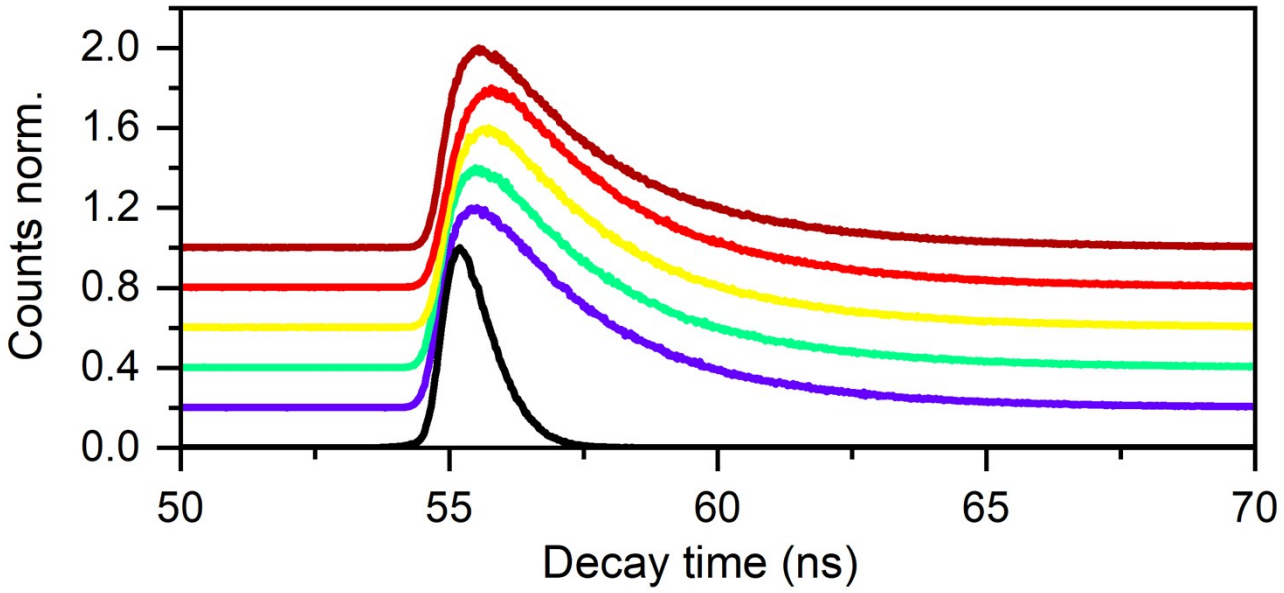

Figure S27: Fluorescence decay time measurements of five different positions of C5 crystals, excited at 520 nm (4.5 nW). The colored curves are the fluorescence decays, while the black curve is the instrument response function (IRF). The C5 crystals measured here were grown with the same conditions as the ones in Figure S23, but are from a different well-plate. Every decay was tail-fitted with 2 exponents, and intensity-weighted average decay times of 2.60, 2.67, 2.63, 2.69, and 2.62 ns were found. The average decay time (2.64 ns) obtained from these five values is used in the manuscript.

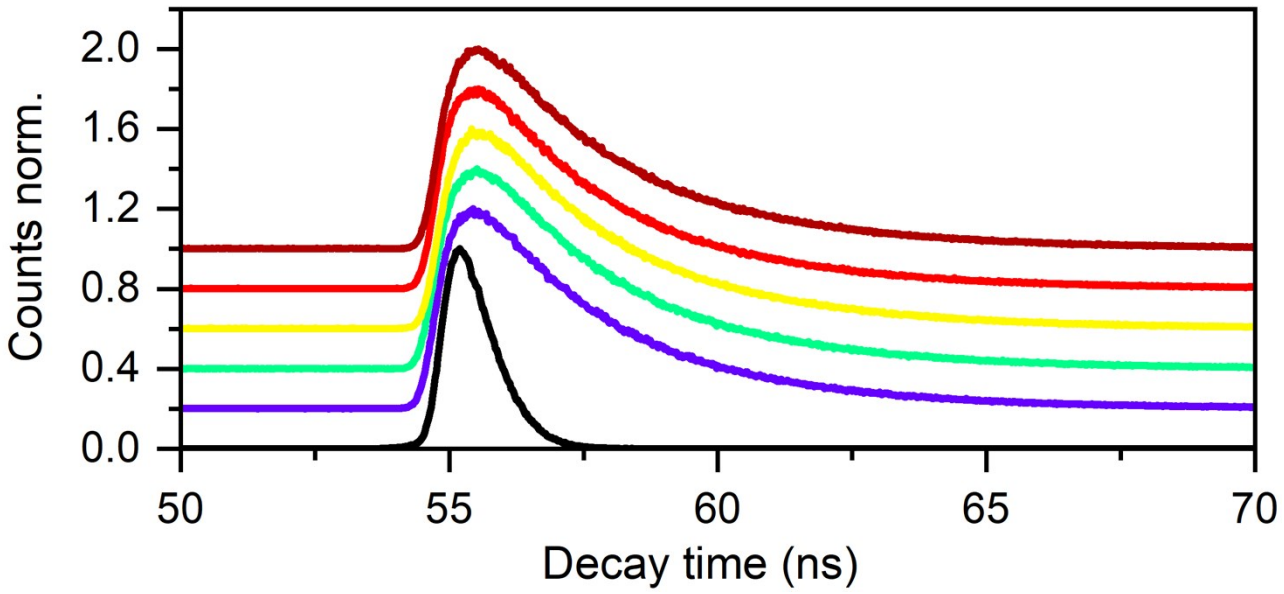

Figure S28: Fluorescence decay time measurements of five different positions of G5-NIR crystals, excited at 520 nm (45 nW). The colored curves are the fluorescence decays, while the black curve is the instrument response function (IRF). Every decay was tail-fitted with 2 exponents, and intensity-weighted average decay times of 2.88, 2.89, 2.91, 2.84, and 2.90 ns were found. The average decay time (2.88 ns) obtained from these five values is used in the manuscript.

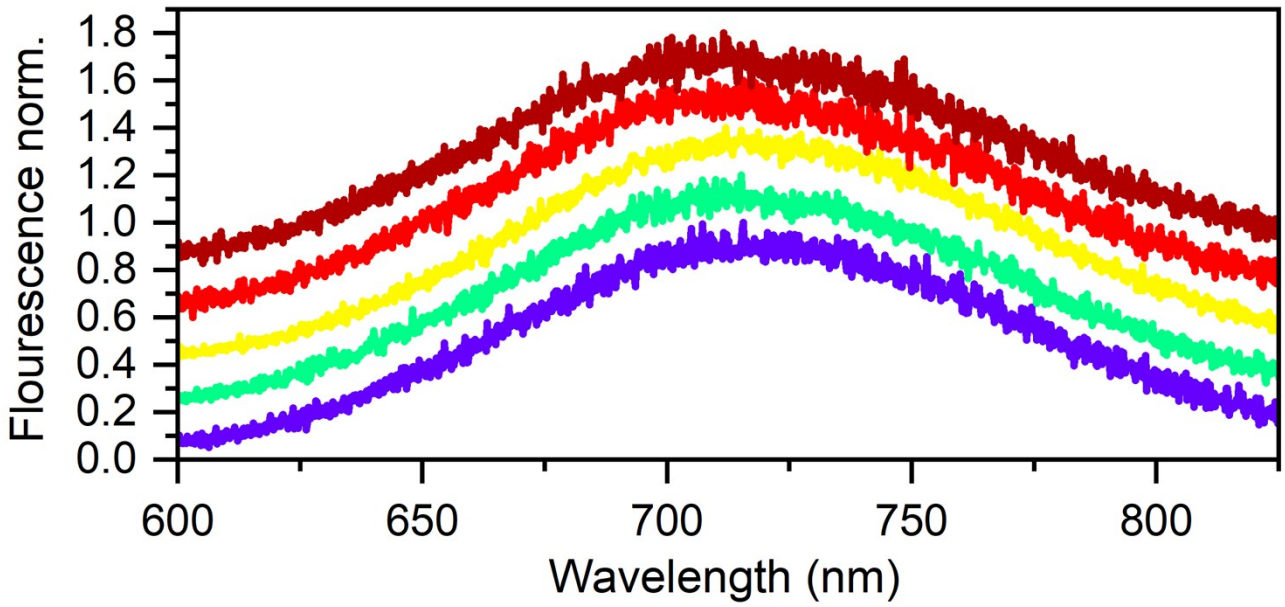

Figure S29. Emission spectra of five different positions of the X5 crystals, excited at 520 nm (450 nW). The spectra are normalized to the emission maximum and have a constant 0.2 offset for displaying purposes.

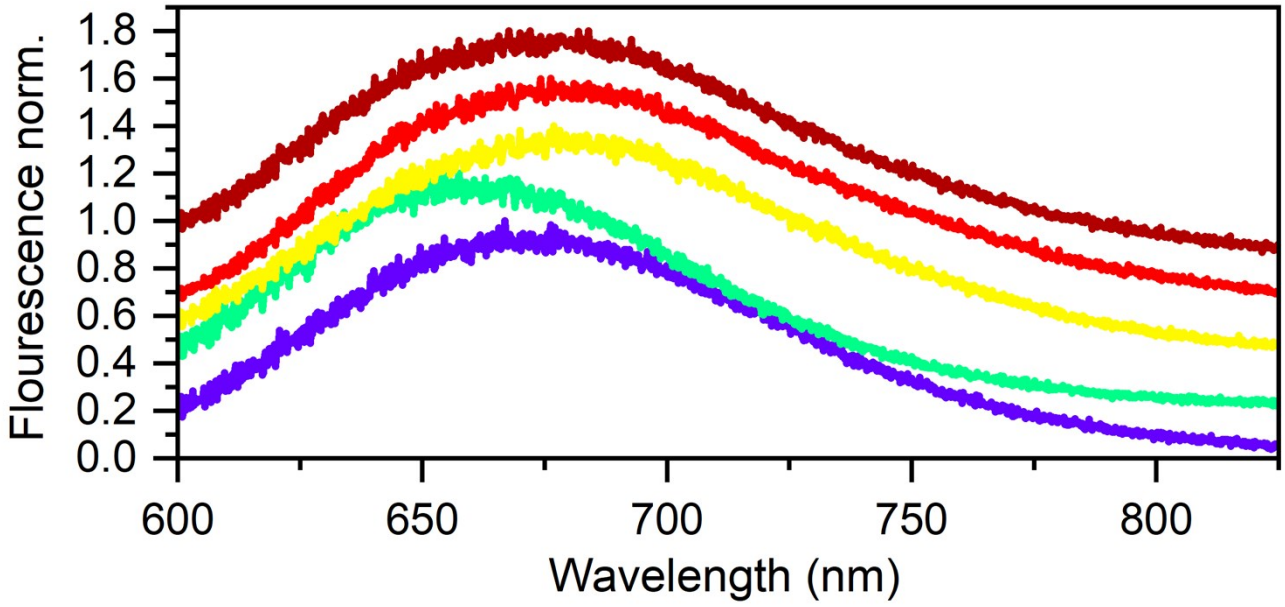

Figure S30. Emission spectra of five different positions of the A5 crystals, excited at 520 nm (450 nW). The spectra are normalized to the emission maximum and have a constant 0.2 offset for displaying purposes.

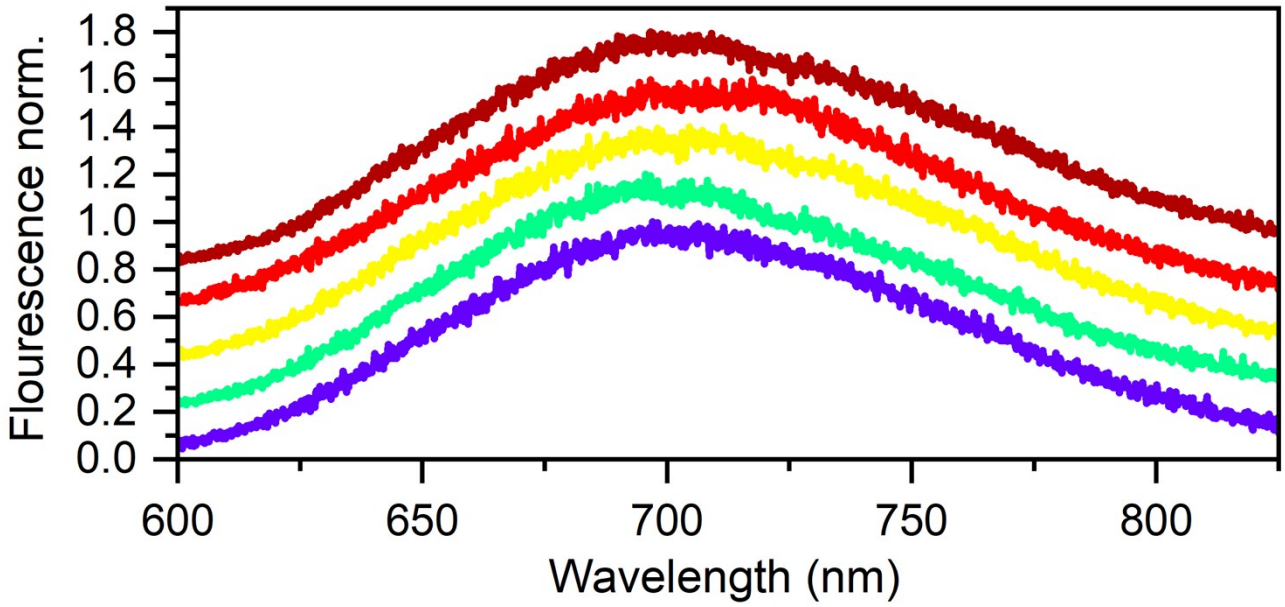

Figure S31: Emission spectra of five different positions of the C5 crystals, excited at 520 nm (45 nW). The spectra are normalized to the emission maximum and have a constant 0.2 offset for displaying purposes. The C5 crystals measured here were grown with the same conditions as the ones in Figure S23, but are from a different well-plate.

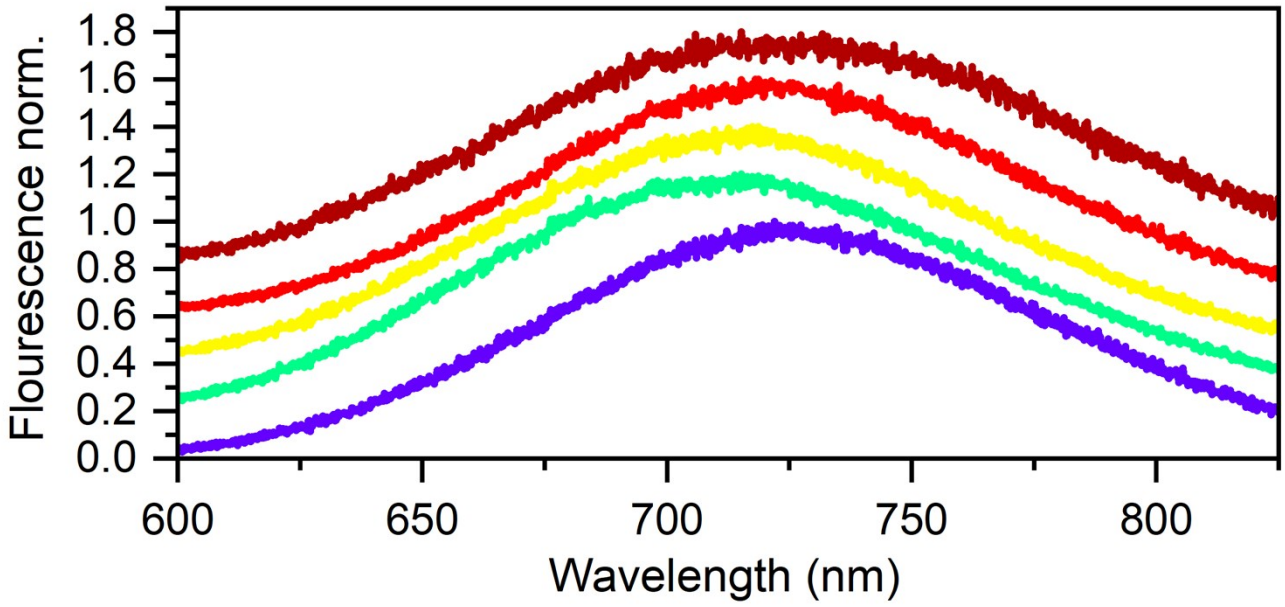

Figure S32. Emission spectra of five different positions of the G5-NIR crystals, excited at 520 nm (450 nW). The spectra are normalized to the emission maximum and have a constant 0.2 offset for displaying purposes.

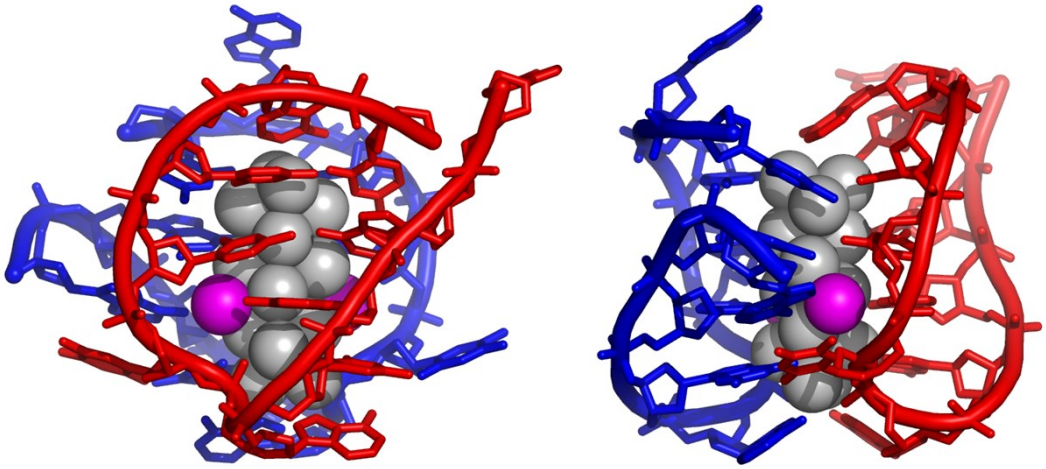

Figure S33. Structure of the original T5 subunit (PDB-ID = 6JR4), front and side views.

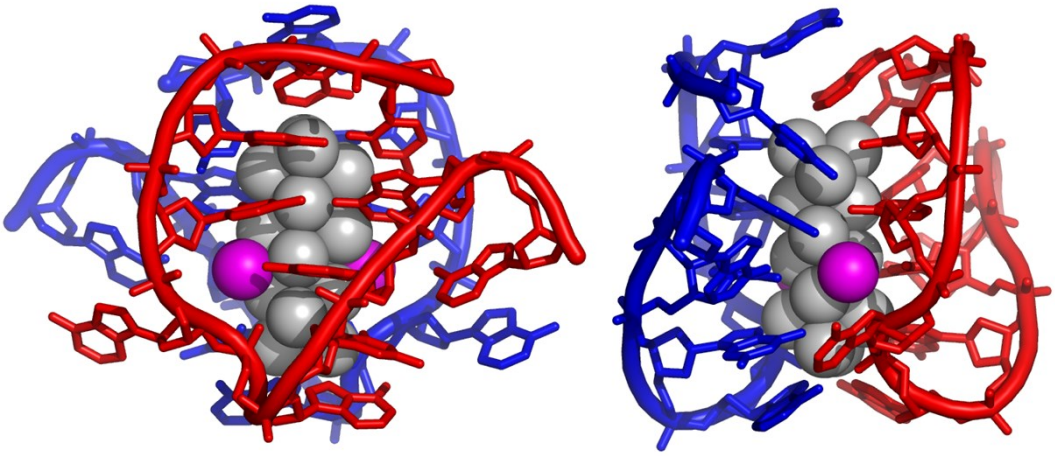

Figure S34. Structure of the A5 subunit (PDB-ID = 7BSE), front and side views.

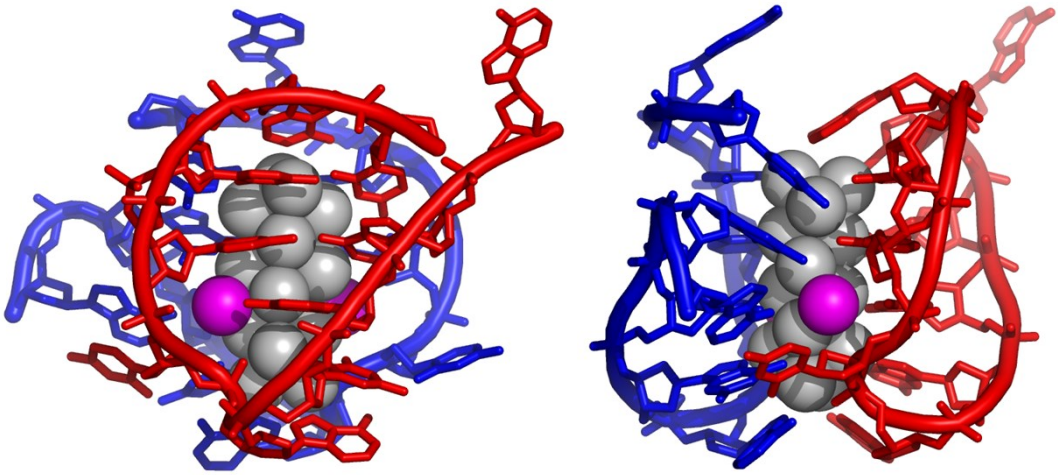

Figure S35. Structure of the C5 asymmetric unit (PDB-ID = 7BSF), front and side views.

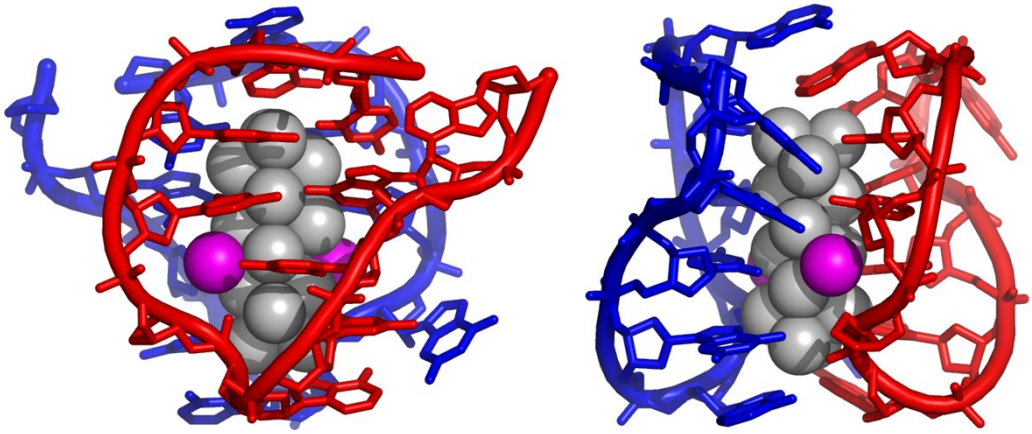

Figure S36. Structure of the G5-NIR asymmetric unit (PDB-ID = 7BSG), front and side views.

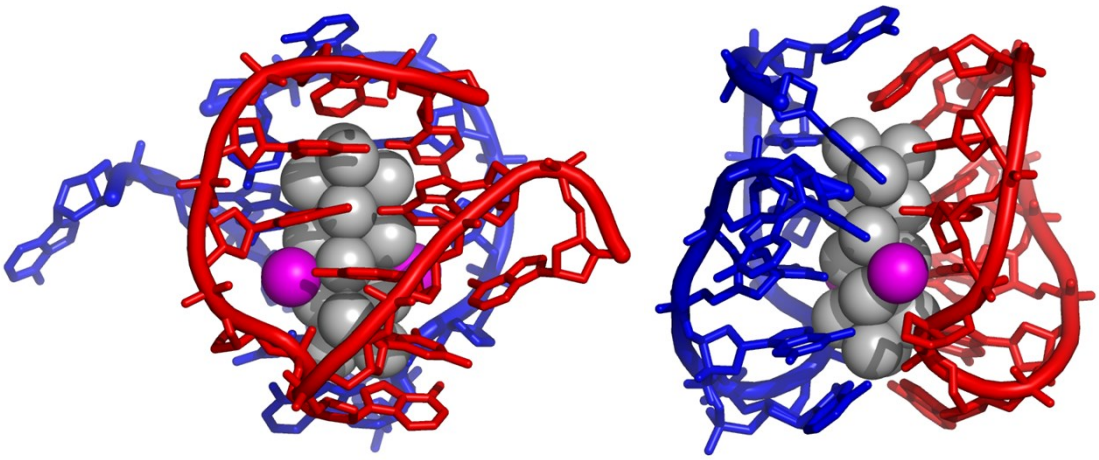

Figure S37. Structure of the X5 asymmetric unit (PDB-ID = 7BSH), front and side views.

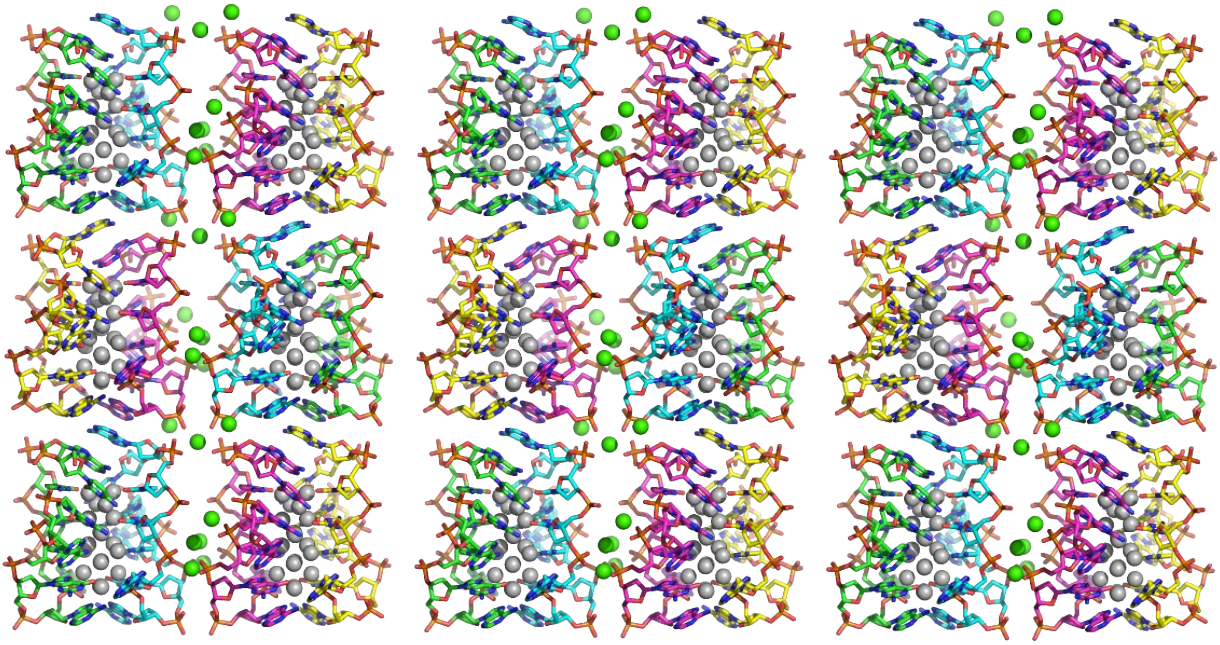

Figure S38. Partial view of the A5 packing in the crystalline state (2 subunits in every asymmetric unit).

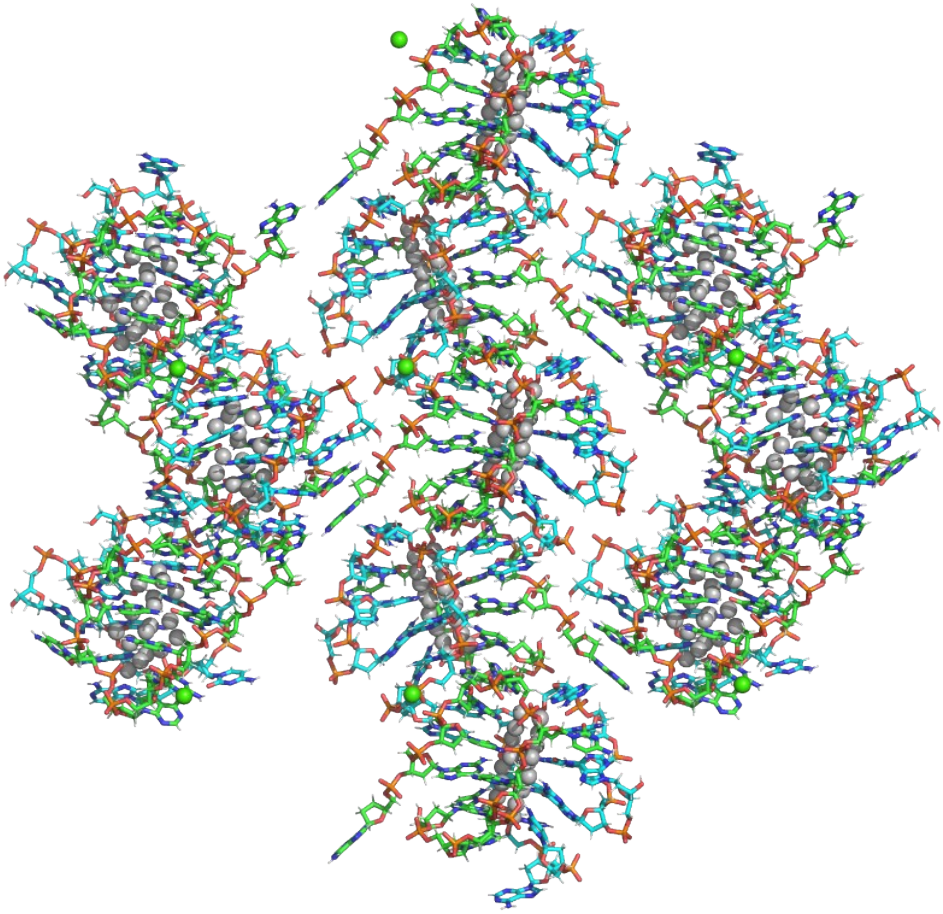

Figure S39. Partial view of the C5 packing in the crystalline state.

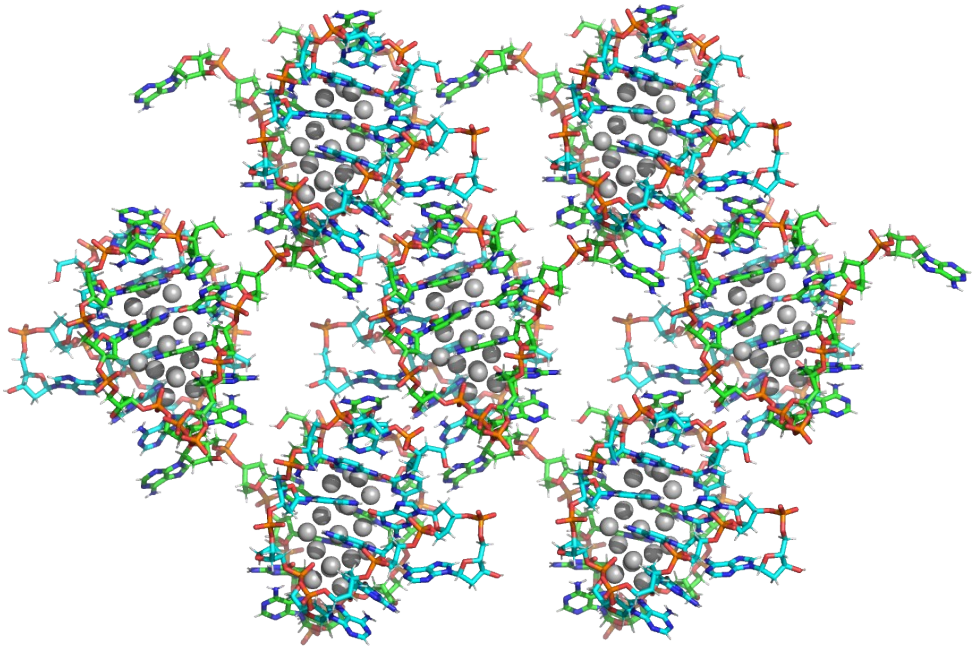

Figure S40. Partial view of the X5 packing in the crystalline state.

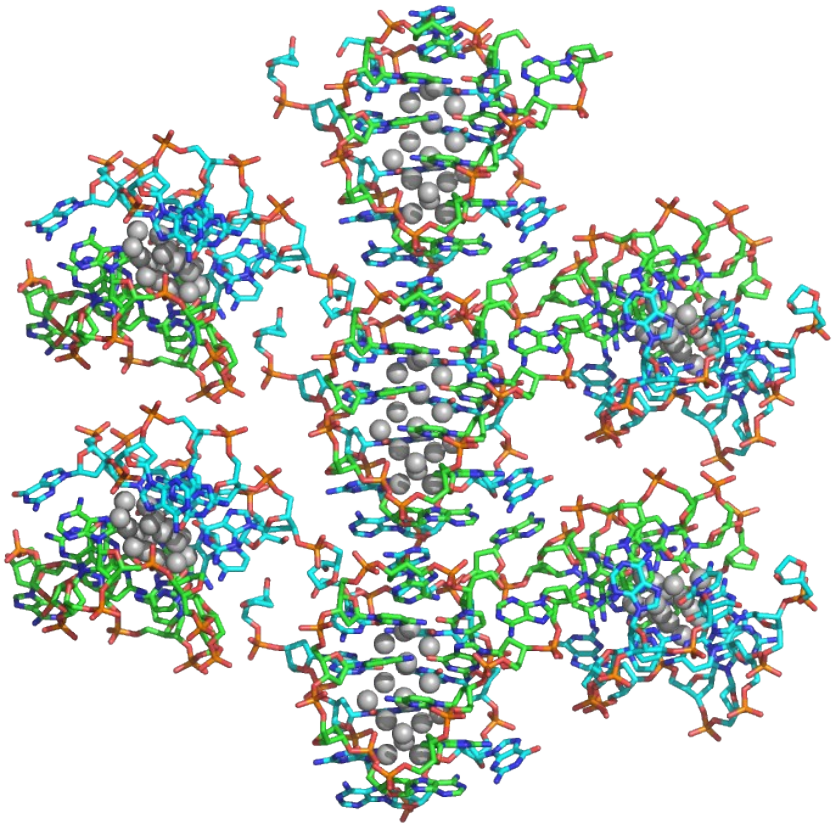

Figure S41. Partial view of the G5-NIR packing in the crystalline state.

Crystal code	A5 mutant	C5 mutant
PDB-ID	7BSE	7BSF
Crystal data		
Space group	$P4_32_12$	$P2_12_12_1$
Unit cell (Å)	$a = b = 45.4$, $c = 82.7$	$a = 24.0$, $b = 33.8$, $c = 52.5$
No. of DNA strands in AU [a]	4	2
No. of Ag atoms in AU [a,1]	32	16
No. of additional Ag^+ positions in AU [a,2]	4	2
No. of Ca^{2+} ions in AU [a,1]	8	1
Data collection		
Beamline	BL-17A in Photon Factory	BL-17A in Photon Factory
Wavelength (Å)	0.98	0.98
Resolution (Å)	32.1-1.5	28.4 – 1.1
of the outer shell (Å)	1.54-1.5	1.13 – 1.1
Unique reflections	26478	33404
Completeness (%)	99.7	99.6
in the outer shell (%)	97.9	97.7
R_{anom} [b] (%)	10.9	8.9
in the outer shell (%)	39.2	27.6
Redundancy	13.9	6.8
in the outer shell	13.8	6.2
$I/\sigma(I)$	17.2	14.1
in the outer shell	7.4	5.4
Structure refinement		
Resolution range (Å)	32.1-1.5	28.4 – 1.1
Used reflections	26283	33403
R-factor [c] (%)	12.4	7.5
R_{free} [d] (%)	13.7	8.3
R.m.s.d. bond length (Å)	0.009	0.010
R.m.s.d. bond angles (°)	1.1	1.3

[a] Number of molecules, atoms or ions in the asymmetric unit.

[b] $R_{merge} = R_{anom} = 100 \times \Sigma_{hklj} | I_{hklj}(+) - I_{hklj}(-) | \; / \; \Sigma_{hklj} [I_{hklj}(+) + I_{hklj}(-)]$.

[c] R-factor $= 100 \times \Sigma | |F_o| - |F_c| | \; / \; \Sigma |F_o|$, where $|F_o|$ and $|F_c|$ are optimally scaled observed and calculated structure factor amplitudes, respectively.

[d] Calculated using a random set containing 10% of observations.

[1] With occupancy 1

[2] With occupancy significantly below 1

Table S3. Crystal data, statistics of data collections and structure refinements for the A5 and C5 mutants.

Crystal code	G5-NIR mutant	X5 mutant
PDB-ID	7BSG	7BSH
Crystal data		
Space group	$C222_1$	$P2_12_12_1$
Unit cell (Å)	a = 29.9, b = 33.7, c = 76.8	a = 28.2, b = 36.0, c = 43.5
No. of DNA strands in AU [a]	2	2
No. of Ag atoms in AU [a,1]	16	16
No. of additional Ag^+ positions in AU [a,2]	2	2
No. of Ca^{2+} ions in AU [a,1]	0	0
Data collection		
Beamline	BL-17A in Photon Factory	BL-17A in Photon Factory
Wavelength (Å)	0.98	0.98
Resolution (Å)	22.4-2.2	27.7-1.2
of the outer shell (Å)	2.25-2.2	1.23-1.2
Unique reflections	3775	26773
Completeness (%)	98.2	99.9
in the outer shell (%)	98.4	99.2
R_{anom} [b] (%)	13.0	6.2
in the outer shell (%)	31.9	29.6
Redundancy	3.1	6.8
in the outer shell	2.7	6.5
$I/\sigma(I)$	5.6	18.8
in the outer shell	2.6	6.2
Structure refinement		
Resolution range (Å)	22.4-2.2	27.7-1.2
Used reflections	3775	26741
R-factor [c] (%)	20.8	7.7
R_{free} [d] (%)	24.7	8.8
R.m.s.d. bond length (Å)	0.013	0.010
R.m.s.d. bond angles (°)	1.4	1.2

[a] Number of molecules, atoms or ions in the asymmetric unit.

[b] $R_{merge} = R_{anom} = 100 \times \Sigma_{hklj} | I_{hklj}(+) - I_{hklj}(-) | / \Sigma_{hklj} [I_{hklj}(+) + I_{hklj}(-)]$.

[c] R-factor $= 100 \times \Sigma | |F_o| - |F_c| | / \Sigma |F_o|$, where $|F_o|$ and $|F_c|$ are optimally scaled observed and calculated structure factor amplitudes, respectively.

[d] Calculated using a random set containing 10% of observations.

[1] With occupancy 1

[2] With occupancy significantly below 1

Table S4. Crystal data and statistics of data collections and structure refinements for the G5-NIR and X5 mutants.

References.

1. Bogh, S. A.; Carro-Temboury, M. R.; Cerretani, C.; Swasey, S. M.; Copp, S. M.; Gwinn, E. G.; Vosch, T., Unusually large Stokes shift for a near-infrared emitting DNA-stabilized silver nanocluster. *Methods and Applications in Fluorescence* **2018,** *6* (2).
2. Brouwer, A. M., Standards for photoluminescence quantum yield measurements in solution (IUPAC Technical Report). **2011,** *83* (12), 2213.
3. Mooney, J.; Kambhampati, P., Get the Basics Right: Jacobian Conversion of Wavelength and Energy Scales for Quantitative Analysis of Emission Spectra. *J. Phys. Chem. Lett.* **2013,** *4* (19), 3316-3318.
4. Carro Temboury, M. R.; Paolucci, V.; Hooley, E. N.; Latterini, L.; Vosch, T., Probing DNA-stabilized fluorescent silver nanocluster spectral heterogeneity by time-correlated single photon counting. *Analyst* **2016,** *141* (1), 123-130.
5. Lakowicz, J. R., *Principles of Fluorescence Spectroscopy*. 3rd ed.; Springer: 2006.
6. Cerretani, C.; Kanazawa, H.; Vosch, T.; Kondo, J., Crystal structure of a NIR-Emitting DNA-Stabilized Ag16 Nanocluster. *Angew. Chem. Int. Ed.* **2019,** *58* (48), 17153-17157.
7. Kabsch, W., Integration, scaling, space-group assignment and post-refinement. *Acta Crystallogr., Sect D: Biol. Crystallogr.* **2010,** *66* (2), 133-144.

8. Liebschner, D.; Afonine, P. V.; Baker, M. L.; Bunkoczi, G.; Chen, V. B.; Croll, T. I.; Hintze, B.; Hung, L.-W.; Jain, S.; McCoy, A. J.; Moriarty, N. W.; Oeffner, R. D.; Poon, B. K.; Prisant, M. G.; Read, R. J.; Richardson, J. S.; Richardson, D. C.; Sammito, M. D.; Sobolev, O. V.; Stockwell, D. H.; Terwilliger, T. C.; Urzhumtsev, A. G.; Videau, L. L.; Williams, C. J.; Adams, P. D., Macromolecular structure determination using X-rays, neutrons and electrons: recent developments in Phenix. *Acta Crystallographica Section D* **2019,** *75* (10), 861-877.
9. McCoy, A. J.; Grosse-Kunstleve, R. W.; Adams, P. D.; Winn, M. D.; Storoni, L. C.; Read, R. J., Phaser crystallographic software. *J. Appl. Crystallogr.* **2007,** *40* (4), 658-674.
10. Emsley, P.; Lohkamp, B.; Scott, W. G.; Cowtan, K., Features and development of Coot. *Acta Crystallogr., Sect D: Biol. Crystallogr.* **2010,** *66* (4), 486-501.
11. Emsley, P.; Cowtan, K., Coot: Model-building tools for molecular graphics. *Acta Crystallogr., Sect D: Biol. Crystallogr.* **2004,** *60* (12 I), 2126-2132.